

Quarterly Report for
Contract DE-FG07-02ID14418
Stanford Geothermal Program
October-December 2002

Table of Contents

1. STEAM-WATER RELATIVE PERMEABILITY IN FRACTURES	1
1.1 THEORETICAL BACKGROUND	1
1.2 LITERATURE REVIEW	3
1.3 PREVIOUS RESULTS OF THE UNSTEADY STEAM-WATER EXPERIMENT	5
1.4 STEADY-STATE EXPERIMENTS	11
1.5 PRELIMINARY RESULTS	17
2. NUMERICAL SIMULATION WITHOUT USING EXPERIMENTAL RELATIVE PERMEABILITY	19
2.1 SUMMARY	19
2.2 INTRODUCTION	19
2.3 THEORY	21
2.3 RESULTS	22
2.5 DISCUSSION	31
2.6 CONCLUSIONS	33
2.7 FUTURE WORK	33
3. REFERENCES	35

1. STEAM-WATER RELATIVE PERMEABILITY IN FRACTURES

This project is being conducted by Research Assistant Chih-Ying Chen, Senior Research Engineer Kewen Li and Prof. Roland Horne. The goal of this research has been to gain better understanding of steam-water transport through fractured media and determine the behavior of relative permeability in fractures. According to the observations of Diomampo (2001), nitrogen-water flow through fractures is described most appropriately by using the porous medium (relative permeability) model. However, from the preliminary results of the unsteady experiment in this research, steam-water flow in fractures shows a different behavior from nitrogen-water flow. The average steam-water relative permeabilities show less phase interference, and behave closer to the X-curve. To confirm this result and obtain more accurate and consistent steam-water relative permeabilities, the steady-state experiments is in progress.

1.1 THEORETICAL BACKGROUND

Multiphase flow is an important mechanism in geothermal reservoirs, which are complex systems of porous and fractured media. Complete understanding of geothermal fluid flow requires knowledge of flow in both media. Normally, fractures are the main conduits for fluid. In geothermal reservoirs, the fluids, steam and water, are both derived from the same substance but in different phases. The phase change during steam-water flow is a physical phenomenon that does not occur in the multiphase flow of distinct fluids such as air and water, hence the multiphase flow properties are likely to differ. At present, the governing flow mechanism for boiling multiphase flow in fractures is still undetermined. There are two approaches commonly used to model multiphase flow in fractures, the porous medium approach and the equivalent homogeneous single-phase approach.

The porous medium approach treats fractures as connected two-dimensional porous media. In this model, a pore space occupied by one phase is not available for flow for the other phase. A phase can move from one position to another only upon establishing a continuous flow path for itself. As in porous media, the competition for pore occupancy is described by relative permeability and governed by Darcy's law. Darcy's law for single-phase liquid system is:

$$u_l = \frac{k_{abs}(p_i - p_o)}{\mu_l L} \quad (1.1)$$

where subscript l stands for the liquid phase, i for inlet and o for outlet; μ , p , L , u , k_{abs} are the viscosity, pressure, fracture length, Darcy flow velocity and absolute permeability respectively. The Darcy flow velocity is equal to

$$u = \frac{q}{bw} \quad (1.2)$$

with q as the volumetric flow rate, b the fracture aperture and w as the fracture width. Absolute permeability of a smooth-walled fracture is a function only of the fracture aperture (Witherspoon et al., 1980) as described in the relationship:

$$k_{abs} = \frac{b^2}{12} \quad (1.3)$$

For liquid phase in two-phase flow, Eq. 1.1 becomes

$$u_l = \frac{k_{abs} k_{rl} (p_i - p_o)}{\mu_l L} \quad (1.4)$$

where k_{rl} is the relative permeability of the liquid phase.

Similarly, Darcy's law derived for single-phase isothermal gas flow in porous media (Scheidegger, 1974) is:

$$u_g = \frac{k_{abs} (p_i^2 - p_o^2)}{2\mu_g L p_o} \quad (1.5)$$

with the subscript g pertaining to the gas phase.

In two-phase flow, Eq. 1.5 becomes

$$u_g = \frac{k_{abs} k_{rg} (p_i^2 - p_o^2)}{2\mu_g L p_o} \quad (1.6)$$

with k_{rg} as the gas relative permeability. The sum of the k_{rl} and k_{rg} indicates the extent of phase interference. A sum of relative permeabilities equal to one means the absence of phase interference. Physically this implies each phase flows in its own path without impeding the flow of the other. The lower is the sum of the relative permeabilities below 1, the greater is the phase interference.

Relative permeability functions are usually taken to be dependent on phase saturation. The two most commonly used expressions for relative permeability for homogeneous porous media are the X-curve and Corey curve (Corey, 1954). The X-curve defines relative permeability as a linear function of saturation:

$$k_{rl} = S_l \quad (1.7)$$

$$k_{rg} = S_g \quad (1.8)$$

where S_l and S_g are the liquid and gas saturation respectively. The Corey curves relate relative permeability to the irreducible or residual liquid and gas saturation, S_{rl} and S_{rg} :

$$k_{rl} = S^{*4} \quad (1.9)$$

$$k_{rg} = (1 - S^*)^2 (1 - S^{*2}) \quad (1.10)$$

$$S^* = (S_l - S_{rl}) / (1 - S_{rl} - S_{rg}) \quad (1.11)$$

The equivalent homogeneous single-phase approach treats flow through fractures as a limiting case of flow through pipes. In this model, phase velocities in the fracture are equal and capillary forces are negligible. A continuous flow path is not required for movement of each phase. A phase can be carried along by one phase as bubbles, slug or other complex structures. As in pipes, flow can be described by the concept of friction factors and using averaged properties (Fourar et al., 1993):

$$\frac{(p_i - p_o)}{L} = \frac{\Pi f \rho_m V_m^2}{2A} \quad (1.12)$$

where Π is the fracture perimeter, A is the cross sectional area to flow, ρ_m average density and V_m as average flow velocity. The average density is described by:

$$\rho_m = \frac{\rho_g q_g + \rho_l q_l}{q_g + q_l} \quad (1.13)$$

The average flow velocity is equal to:

$$V_m = \frac{q_g + q_l}{A} \quad (1.14)$$

The friction factor, f , is derived empirically as a function of the averaged Reynolds number calculated by:

$$N_{Re} = \frac{2bV_m\rho_m}{\mu_m} \quad (1.15)$$

with μ_m as average viscosity:

$$\mu_m = \frac{\mu_g q_g + \mu_l q_l}{q_g + q_l} \quad (1.16)$$

There are several expressions used to relate friction factor and Reynold's number. The commonly used one for flow through fracture is the generalized Blasius form (Lockhart and Martinelli, 1949):

$$f = \frac{C}{N_{Re}^n} \quad (1.17)$$

with C and n as constants derived from experimental data.

According to the results from Diomampo (2001), nitrogen-water flow through fractures is described more appropriately by using the porous medium (relative permeability) approach based on the observations of the multiphase flow behavior. However in the steam-water case, the applicability of the two models for multiphase flow through fractures is still undetermined. From the preliminary results in this research, the steam-water flow shows a different behavior from the nitrogen-water case reported by Diomampo (2001).

1.2 LITERATURE REVIEW

The fluids in geothermal reservoirs, steam and water, are both derived from the same substance. However, they form different phases. The phase change during steam-water multiphase flow has made it difficult to investigate steam-water relative permeability. Even in multiphase flow without boiling, only a few published data are available for two-phase flow in fractures. Most of the studies have been done for air-water systems or for water-oil systems.

Earliest is Romm's (1966) experiment with kerosene and water through an artificial parallel-plate fracture lined with strips of polyethylene or waxed paper. Romm found a linear relationship between permeability and saturation, $S_w = k_{rw}$, $S_{nw} = k_{rnw}$ such that $k_{rw} + k_{rnw} = 1$ which represents the X-curve behavior. Fourar et al. (1993) artificially roughened glass plates with beads and flowed an air-water mixture between them. Fourar and Bories (1995) did similar experiments using smooth glass plates and clay bricks. Both

studies observed flow structures like bubbles, annular and fingering bubbles comparable to flow in pipes and depicted flow in fractures to be better correlated using the equivalent homogeneous single-phase model. Pan et al. (1996) observed the identical flow structures in their experiments with an oil-water system. They observed that a discontinuous phase can flow as discrete units along with the other phase. Pan et al. (1996) also found their experimental pressure drop to be better predicted by a homogenous single-phase model. All of these experiments showed significant phase interference at intermediate saturations.

Pruess and Tsang (1990) conducted numerical simulation of flow through rough-walled fractures. They modeled fractures as two-dimensional porous media with apertures varying with position. Their study showed the sum of the relative permeabilities to be less than 1, the residual saturation of the nonwetting phase to be large and phase interference to be greatly dependent on the presence or absence of spatial correlation of aperture in the direction of flow. Persoff et al. (1991) did experiments on gas and water flow through rough-walled fractures using transparent casts of natural fractured rocks. The experiment showed strong phase interference similar to the flow in porous media. The relative permeability data of Persoff (1991) and Persoff and Pruess (1995) for flow through rough-walled fractures were compared in Horne et al. (2000) against commonly used relative permeability relations for porous media, the X-curve and Corey curve, as shown in Figure 1.1. Diomampo (2001) performed experiments of nitrogen and water flow through both smooth- and rough-walled artificial fractures, leading to results that are also included in Figure 1.1.

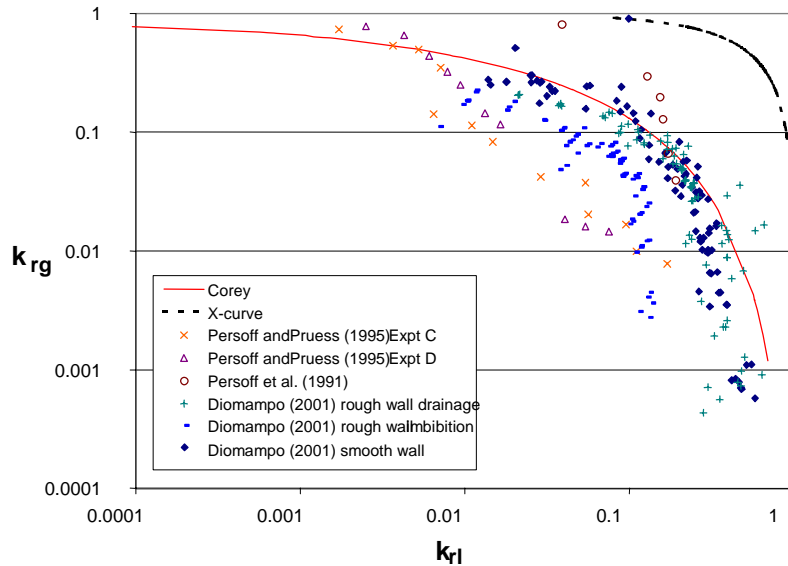


Figure 1.1: Compendium of previous measurements of air-water relative permeabilities in fractures (from Diomampo, 2001).

In the experiments of both Persoff (1991) and Persoff and Pruess (1995), flow of a phase was characterized by having a localized continuous flow path that is undergoing blocking and unblocking by the other phase. Recent parallel plate experiments by Su et al. (1999) illustrate the same flow mechanism of intermittent localized fluid flow. Kneafsy and

Pruess (1998) observed similar intermittent flow in their experiments with pentane through various parallel plate models made from glass, sandblasted glass or transparent fracture replicas. Diomampo (2001) also observed the intermittent phenomenon in her experiments. Furthermore, the results from Diomampo (2001) conform mostly to the Corey type of relative permeability curve (Figure 1.1). This suggests that flow through fractures can be analyzed by treating it as a limiting case of porous media flow and by using the relative permeability approach. These observations are contrary to the findings of Fourar et al (1993), Fourar and Bories (1995), and Pan et al. (1996).

Presently, the flow mechanism and the characteristic behavior of relative permeability in fractures are still not well determined. Issues such as whether a discontinuous phase can travel as discrete units carried along by another phase or will be trapped as residual saturation as in porous medium are unresolved. The question of phase interference i.e. whether the relative permeability curve against saturation is an X-curve, Corey or some other function, is still unanswered. The main objective of this study is to contribute to the resolution of these issues. Experiments on flow through smooth-walled and rough-walled fractures without boiling have been conducted by Diomampo (2001), who established a reliable methodology for flow characterization and relative permeability calculation for nitrogen-water flow. Currently, steam-water system experiments are in progress.

1.3 PREVIOUS RESULTS OF THE UNSTEADY STEAM-WATER EXPERIMENT

A short review of previous results of the unsteady steam-water relative permeability experiment is presented here. For the details of this experiment and its methodology, please refer to the previous quarterly report.

Steam- and Nitrogen-Water Flow Behaviors

A drainage steam-water flow experiment through a smooth-walled fracture has been conducted. The video images have been analyzed, and the corresponding saturations have been obtained satisfactorily. As observed from the video record, the steam-water flow behavior in the fracture is significantly different from the nitrogen-water flow behavior described by Diomampo (2001) in the same fracture. Figure 1.2 shows four consecutive images (under high water saturation) taken when the water injection rate was 2 ml/min, temperature was 102°C, and pressure was around 16.5 psia. The steam (dark part) never forms a stable path or channel, but behaves like moving fingers, slugs and bubbles. These physical phenomena are different from those observed in nitrogen-water flow by Diomampo (2001) as shown in Figure 1.3 which shows that nitrogen forms a nearly stable path.

Comparing Figure 1.2 to Figure 1.3, there is less steam phase near the inlet (the left side) in the steam-water flow in comparison to the nitrogen phase near the inlet in nitrogen-water flow. This is because of the phase transformation from water to steam as pressure decreases in the steam-water flow. Hence the farther the water flows, the more steam it produces. This will be an important factor affecting the steam-water flow behavior under high water saturation situations (>65%). Figure 1.4 shows the steam-water flow under low water saturation (<15%). In this case, it is water that behaves like moving fingers, slugs (the white circle in Figure 1.4) and bubbles. These physical phenomena are different from

those observed by Diomampo (2001) in nitrogen-water flow. According to these preliminary findings, the steam-water flow in fractures might be more suitably described by the equivalent homogeneous single-phase approach.

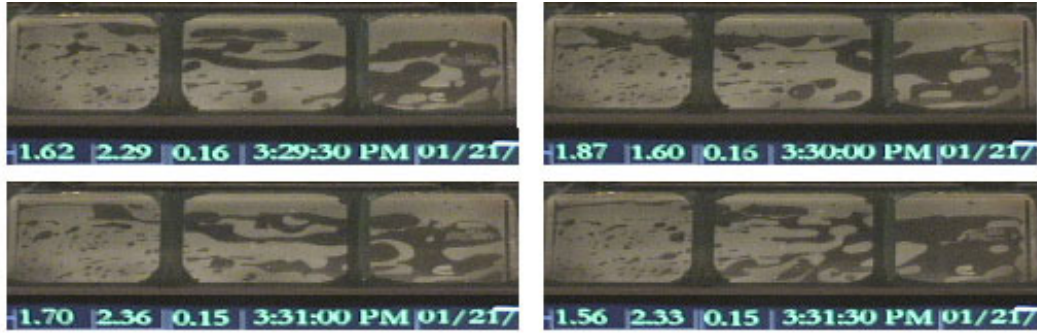


Figure 1.2: The continuous steam-water flow behavior in smooth-walled fracture under high water saturation (>65%) (steam phase is dark, water phase is light).

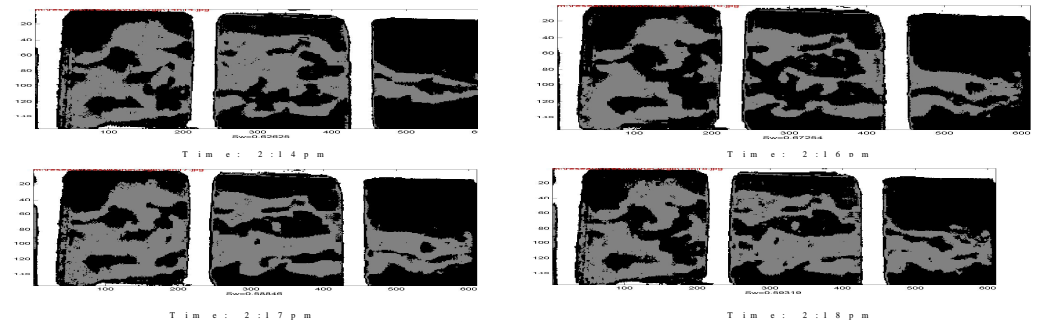


Figure 1.3: The continuous nitrogen-water flow behavior in smooth-walled fracture. Images showing the forming and breaking of gas flow path (light part) (images from Diomampo, 2001).

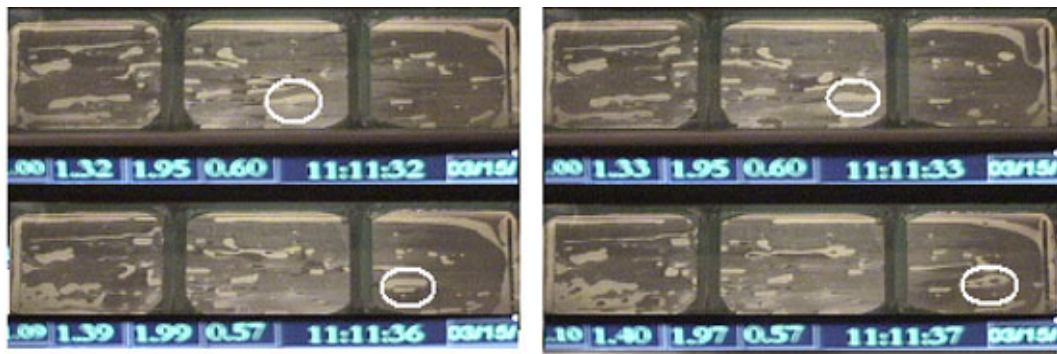


Figure 1.4: The continuous steam-water flow behavior in smooth-walled fracture under low water saturation (<15%). (steam phase is dark, water phase is light).

Unsteady Steam-Water Relative Permeability Experiment

The procedure and detail of the unsteady steam-water relative permeability experiment were described in the previous quarterly report. Figure 1.5 shows the unsteady experiment result. The k_{rw} curve behaves smoothly, whereas the k_{rs} curve is very scattered. As

mentioned before, this scattered effect may be partly associated with the steam and water flow rate measurement error but seems to be caused more prominently by the fluctuating nature of the flow. The detail of this error is due to the delay of f_s and f_w measurement from the FFRD and the measurement error caused by extremely high-speed steam flow which collapses the water component into many tiny water drops that are hard to detect in the FFRD. This will lower the measurement accuracy significantly.

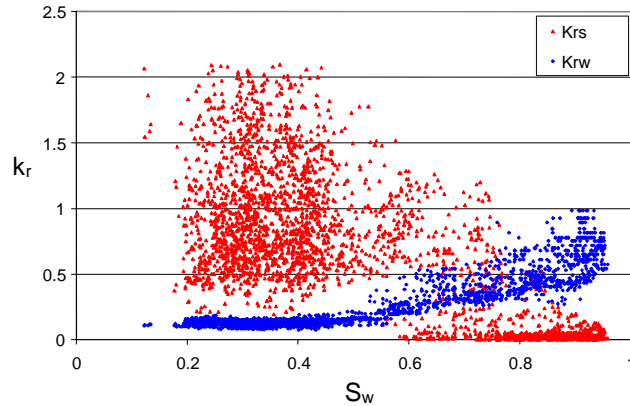


Figure 1.5: Steam-water relative permeability in the unsteady experiment.

Further processing was applied to Figure 1.5 to characterize the steam-water flow behavior. Figure 1.6 was obtained by averaging the relative permeability over 2% saturation ranges from Figure 1.5. The figure shows good correlation in both steam and water curves. What is interesting is that the sum of these two curves is close to 1 which indicates less phase interference. This result is different from the nitrogen-water relative permeabilities which showed a near Corey-type relative permeability behavior. Figure 1.7 shows the comparison of steam-water and nitrogen-water relative permeability curves. The nitrogen-water experiment was conducted by Diomampo (2001) who used the same fracture apparatus but at room temperature. The liquid curves have almost identical trends except in low water saturation range where the steam-water case may lose some accuracy because of the error from the FFRD. On the other hand, the gas curves behave very differently. The steam curve shows a much more mobile character than the nitrogen curve, which can be seen from the higher relative permeability values in the steam curve. This phenomenon was also observed from the digital images.

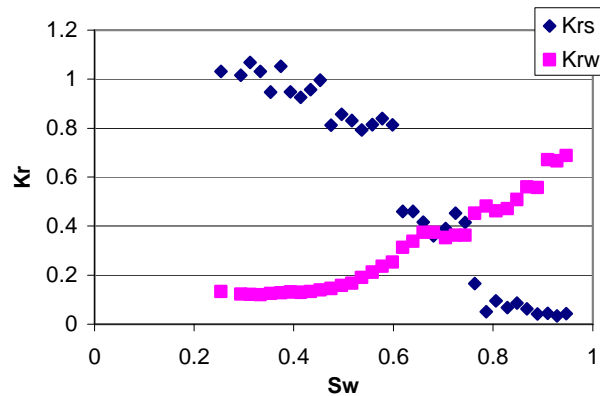


Figure 1.6: Steam-water relative permeabilities in the unsteady experiment by using 2% S_w averages.

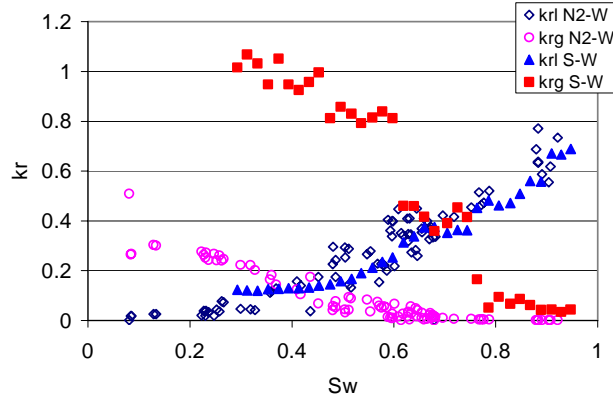


Figure 1.7: Comparison of relative permeability curves between steam- and nitrogen-water cases in the smooth-walled fracture.

Figure 1.8 compares this result with previous research into air-water relative permeabilities in fractures. Most of these studies proposed that the air-water relative permeabilities in fractures follow Corey-type curves or below. However, as can be seen in Figure 1.8, the steam-water relative permeabilities behave closer to the X-curve.

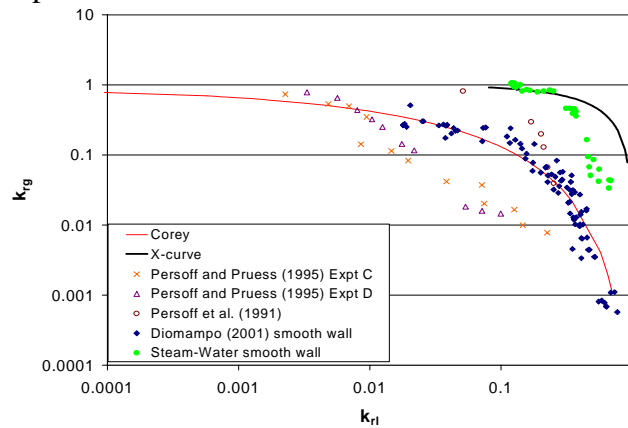


Figure 1.8: Comparison of steam-water relative permeability with previous measurements of air-water relative permeabilities in fractures.

Application of Equivalent Homogeneous Single-Phase Approach for Smooth-Walled Fracture in Unsteady Experiment

The homogeneous single-phase pipe flow model was also applied to the data for the smooth-walled fracture in this unsteady experiment. The calculated friction factor with the modified Reynold's number in log-log plot is shown Figure 1.9. From the fitted linear equation, the constants C and n in Eq. 1.17 are 18 and 1.1 respectively. Figure 1.10 compares this result to previous works for parallel plate experiments. The slope of the fitted line, -1.1, is close to the usual finding of negative unit slope for laminar flow. Also among all the studies, the data are closer to those of Fourar & Bories (1995).

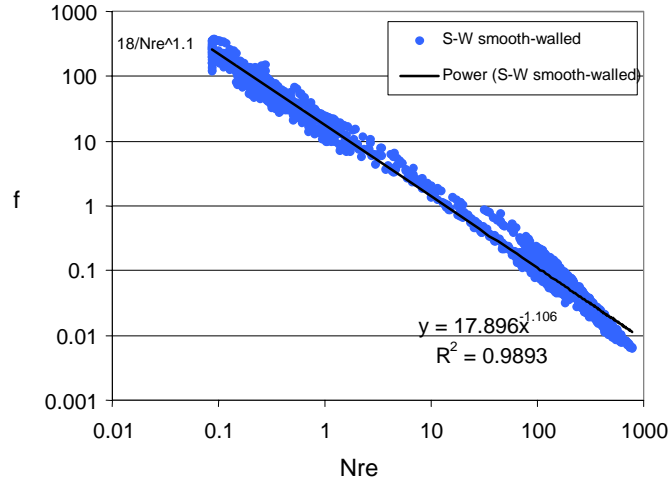


Figure 1.9: Logarithm of friction factor with logarithm of Reynold's number from data of the smooth-walled fracture in unsteady, steam-water experiment.

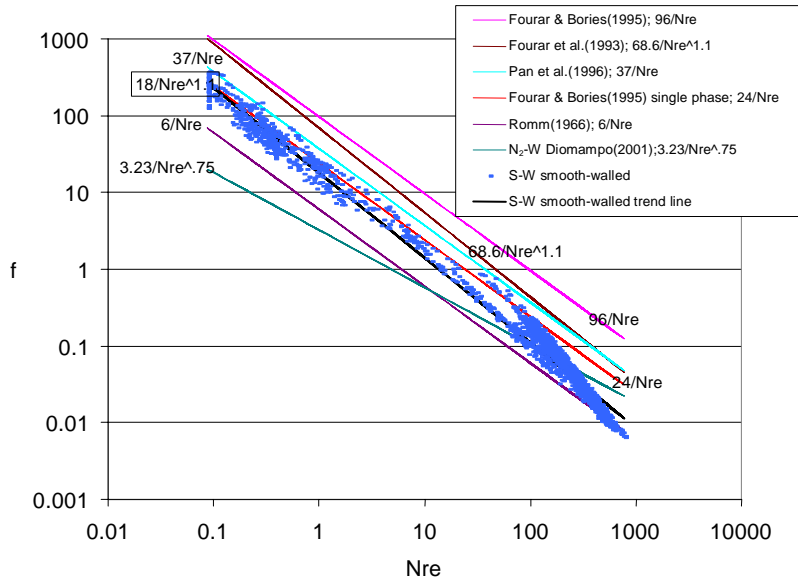


Figure 1.10: Friction Factor against modified Reynold's number for smooth-walled fracture in comparison to previous works.

From Figure 1.10, the C value (from Eq. 1.17) in the fitting curve of the unsteady, steam-water experiment is 18 which is close to the value of single-phase (water) flow in smooth-walled fractures reported by Fourar & Bories (1995) (their value is 24). If only two-phase flow cases are considered, the C value in the unsteady, steam-water experiment is close that of Pan et al. (1996) (their value is 37), which was obtained from the oil-water flow in a smooth-walled fracture. The n value (from Eq. 1.17) in the fitting curve of the unsteady, steam-water experiment is 1.1 which is exactly the same as the value for the air-water flow in a smooth-walled fracture presented by Fourar (1993) and close to all other researchers who suggested an n value of unity. Overall the fit of friction factor as a function of Reynold's number with the steam-water experimental data shows consistency with previous research except that done by Diomampo (2001).

As mentioned in the section on theoretical background, the equivalent homogeneous single-phase approach treats flow through fractures as a limiting case of flow through pipes. As in pipes, the relationship of the pressure drop and friction factor can be described by Eq. 1.12. The pressure drop calculated from Eq. 1.12 in this unsteady, steam-water experiment is depicted in Figure 1.11. The data in Figure 1.11 again are scattered; however the trend line is very close to the 45° line. As in the porous medium model, a 0.001psi range was taken for averaging the data in Figure 1.11. Figure 1.12 shows the averaged results which demonstrate good linearity and mostly follow the 45° line. However the scattered plot in Figure 1.11 shows the same phenomenon as the result obtained from the porous medium model in Figure 1.23. Therefore, the conclusion of which model represents steam-water flow best will not be drawn before the steady, steam-water experiments are finished.

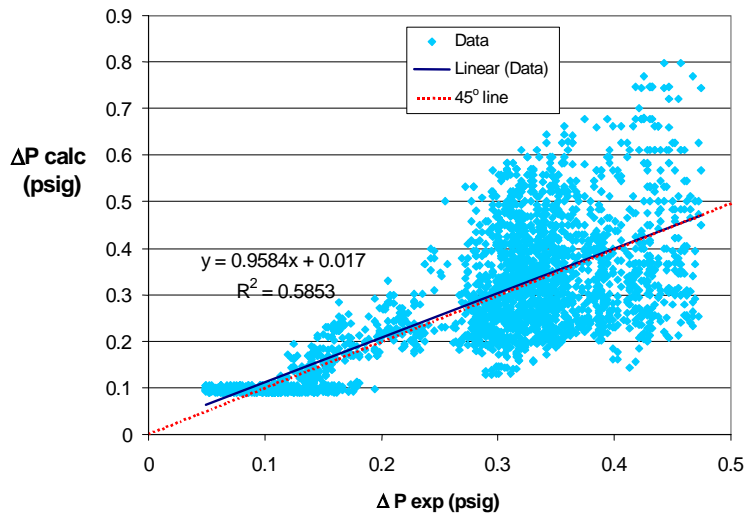


Figure 1.11: Comparison of the predicted pressure drop from homogeneous model and measured data for smooth-walled fracture in unsteady, steam-water experiment.

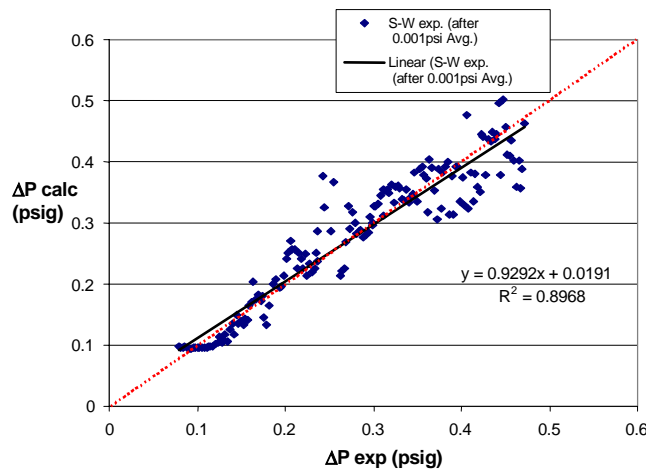


Figure 1.12: Calculated pressure drop from homogeneous model versus measured data for smooth-walled fracture in unsteady, steam-water experiment by using 0.001 psi averages.

Based on the previous unsteady experiment, the following preliminary conclusions may be drawn:

1. The steam-water flow behavior in fractures is different from that of nitrogen-water flow. According to the observations of the steam-water flow video, the steam-water flow in fractures is closer to the homogeneous single-phase behavior.
2. When applying the porous medium approach to model steam-water flow in fractures, scattered steam-phase relative permeability values were obtained, which may be due either to the error of steam and water flow rate measurement and calculation or to the unsteady nature of steam-water flow.
3. The average steam-water relative permeabilities show less phase interference in comparison to the nitrogen-water cases reported by Diomampo (2001). Also, comparing with previous research into air-water relative permeabilities in fractures, the average steam-water relative permeabilities behave closer to the X-curve.
4. When applying the equivalent homogeneous single-phase approach to model steam-water flow in fractures, the modified Reynold's number and friction factor show good consistency with some previous research. However, scattered values of the predicted pressure drop from homogeneous model versus measured pressure drop were obtained, which may be also due to the same reason as described in point 2.

1.4 STEADY-STATE EXPERIMENTS

New experiments will focus on steady-state flow and on improving the accuracy of the measurements. Consistent and repeatable results should be obtained to confirm the steam-water flow behavior in fractures. In order to compare steam-water and nitrogen-water behavior, a nitrogen-water relative permeability experiment is first being conducted under similar conditions to the steam-water experiment (high temperature, similar flow rates and identical analysis method). The detailed design and expected improvement of the steady experiment are described in the following sections.

Improvement of Flow Rate Measurements

As mentioned earlier, the flow rate measurement may contribute one of the major errors in the relative permeability calculation. After reviewing the unsteady experiments done so far, we discovered that our FFRD was not sufficiently sensitive to capture the fractional flow of water, f_w , under high steam-water ratio conditions. According to the previous experiment and calculation, when steam phase relative permeability, k_{rs} , is 0.75, the water fractional flow, f_w , needed is only 0.01. By using the old FFRD and data acquisition system, the detected limit of f_w would only be around this magnitude, which means that when k_{rs} is more than 0.75, we may have a higher likelihood of obtaining inaccurate k_{rs} values due to the inaccuracy of the f_w measurements. This may be another factor that contributes to the scattered results in the plot of steam-water relative permeabilities and the plot of predicted pressure drop against measured pressure drop (beyond the inherently unsteady nature of the flow).

Since the previous report, a narrower transparent glass tubing (3 mm OD, 1.4 mm ID) has been installed to replace the old tubing (3 mm OD, 1.65 mm ID). A new, high-speed data

acquisition board (NI PCI-6023E) was also installed in the data acquisition computer. This replacement increased the data logging frequency from 50Hz to 250Hz. The calibration of water-phase flow rate is shown in Figure 1.13. Though this replacement improved the f_w detection limit of the FFRD from 0.01 to around 0.005, f_w values show erratic and inconsistent behavior when f_w is less than 0.005, as shown in Figure 1.13(b). In order to find the solution to this problem, we observed the actual flow phenomena through the FFRD tubing, and did a preliminary classification of flow patterns correspond to logged FFRD signals. The flow patterns inside the FFRD tubing can be classified into four phenomena. With the increasing of the gas rate, the four phenomena are: segment flow, mostly segment flow, mostly droplet flow, and droplet flow. Cartoons of these four flow patterns are shown in Figure 1.14. The FFRD signals obtained from these four patterns are shown in Figure 1.15.

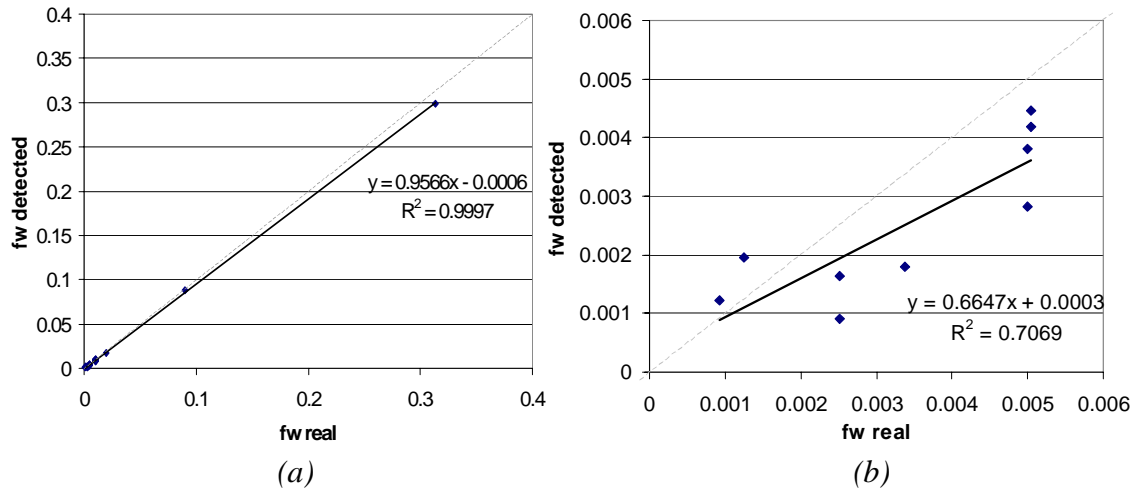


Figure 1.13: FFRD calibration with tubing ID: 1.4mm, (a) large scale, (b) small scale.

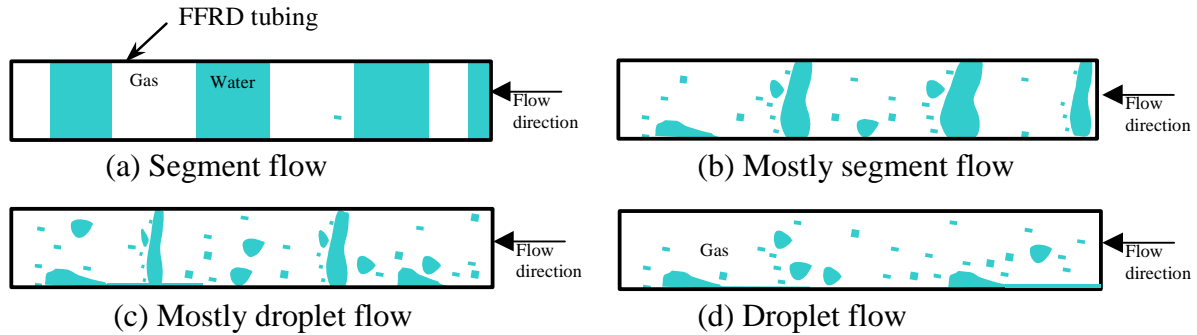


Figure 1.14: Flow pattern cartoons observed from FFRD tubing, (a) segment flow signal, (b) mostly segment flow signal, (c) mostly droplet flow signal and (d) pure droplet flow signal.

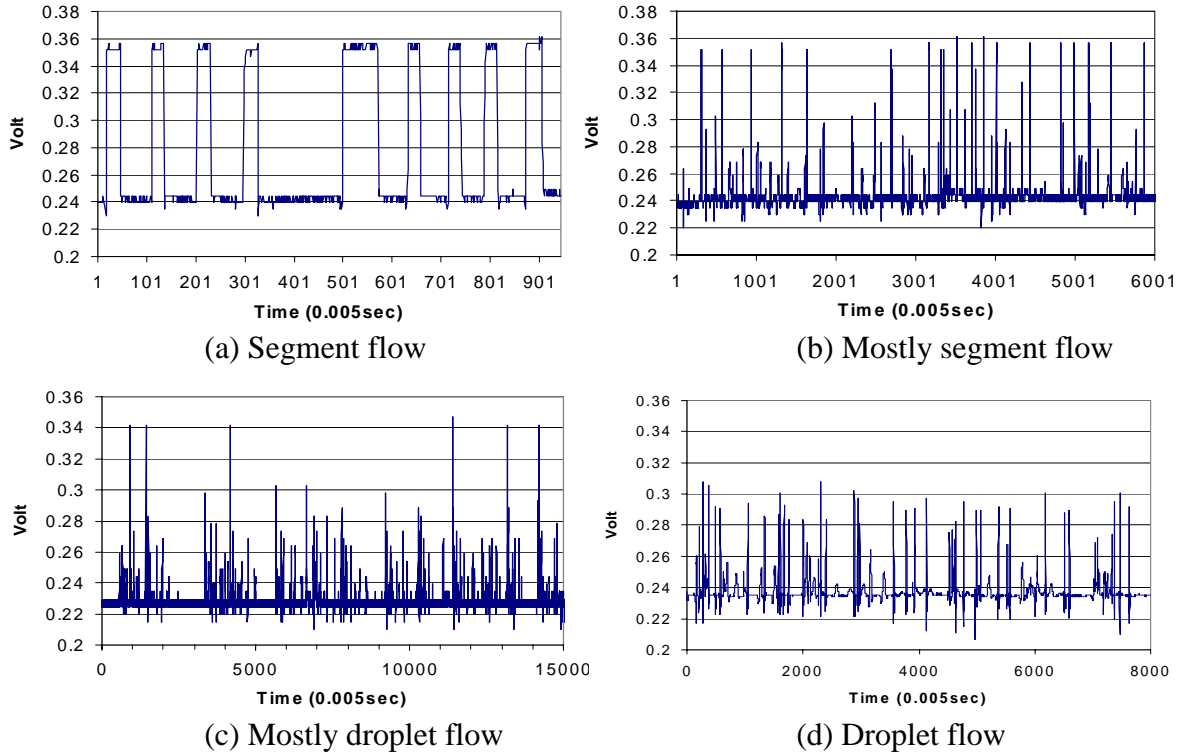


Figure 1.15: FFRD signals correspond to flow patterns shown in figure 1.14, (a) segment flow signal, (b) mostly segment flow signal, (c) mostly droplet flow signal and (d) pure droplet flow signal.

After analyzing all the FFRD signals obtained by using the 1.4mm ID FFRD tubing, the approximate flow pattern map was drawn (Figure 1.16). Comparing Figure 1.16 and Figure 1.13, we discovered that when f_w is less than 0.005, the flow pattern turns to the pure droplet flow. The more the droplet flow, the more error would be obtained in FFRD detection. Droplets inside the tubing reflect and refract the light from the LCD source randomly, hence the signal attenuation becomes nonlinear. Figure 1.13(b) shows this inaccurate indication due to the droplet flow.

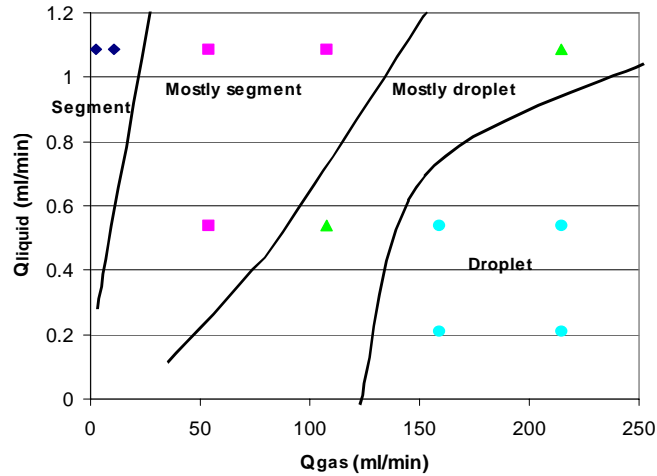


Figure 1.16: Flow pattern map developed from FFRD signal response by using 1.4mm FFRD tubing.

The major factor that controls the flow pattern is FFRD tubing diameter. To avoid the droplet flow, a narrower tubing could be used; however, the narrower the tubing, the more pressure drop throughout the FFRD and the more capillary effect. To maintain an appropriately small pressure drop, keep the tubing size small, and minimize the capillary effect, a new FFRD tubing with 1mm inner diameter and wide-open ends was redesigned to replace the original FFRD tubing (1.4mm) to achieve more segment flow instead of droplet flow inside the FFRD tubing under high flow rates. The schematic of this bell-end tubing is shown in Figure 1.17.

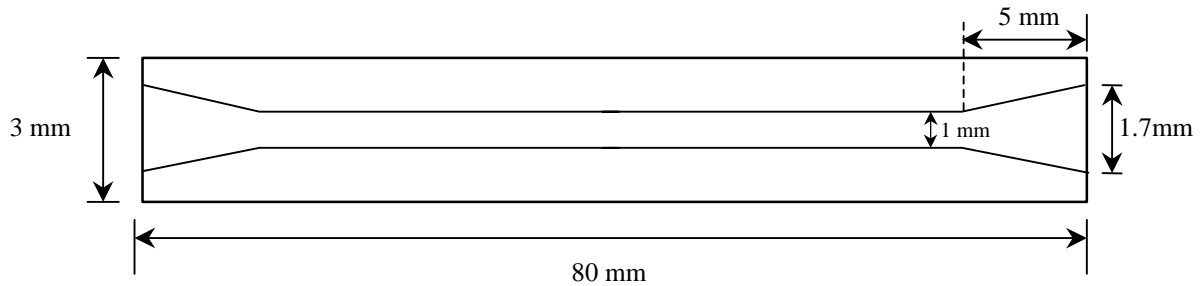


Figure 1.17: Bell-end FFRD tubing (ID=1.0mm, OD=3.0mm, Length=80mm)

The same high-speed data logging program which could reach 250Hz logging frequency was used. Also a more stable DC power supply was installed to avoid signal drift and fluctuation. The new calibration of the FFRD with all the improvements is shown in Figure 1.18 and the new flow pattern map obtained from FFRD signals in different phase-rate ratios is shown in Figure 1.19. Comparing Figure 1.18(b) with Figure 1.13(b), a more accurate measurement of fractional flow in two-phase flow is achieved. This improvement can be explained easily by comparing the flow pattern map in Figure 1.19 with that in Figure 1.16. There is no pure droplet flow region by using this narrower tubing. This increases the accuracy of FFRD logging.

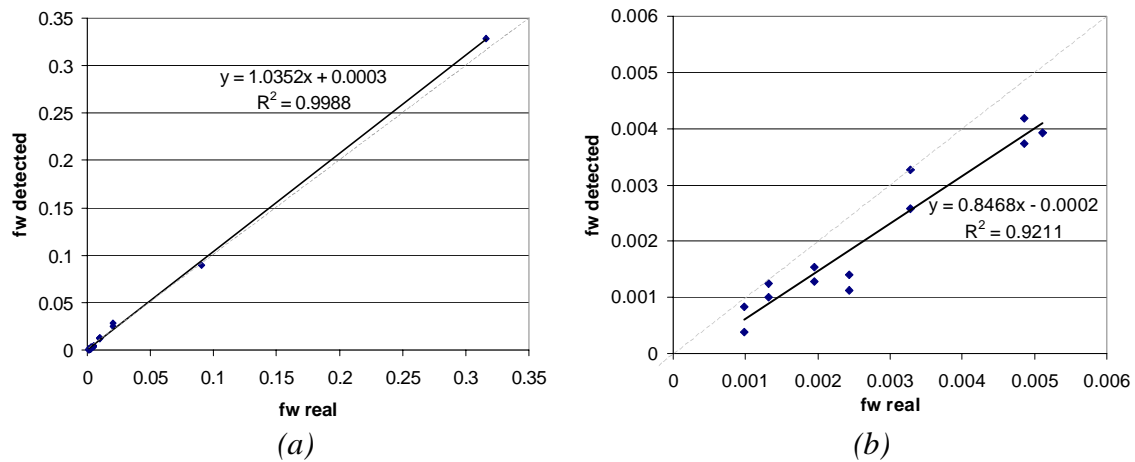


Figure 1.18: FFRD calibration with tubing ID: 1.0mm, (a) large scale, (b) small scale.

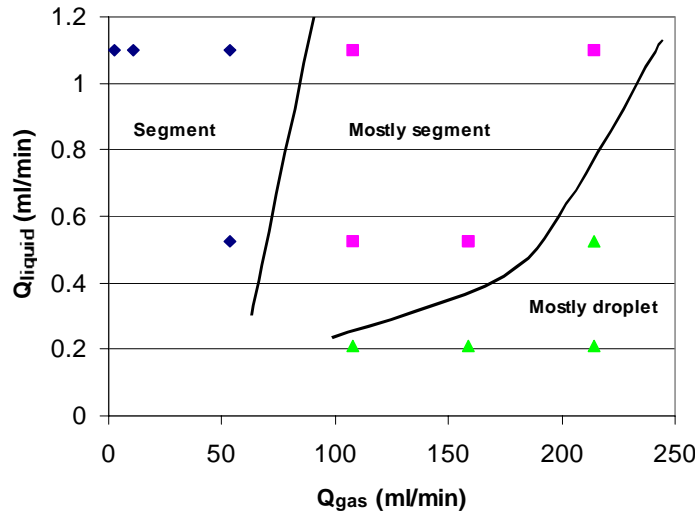


Figure 1.19: Flow pattern map developed from FFRD signal response by using 1.0mm, bell-end FFRD tubing.

Improvement of the Pressure Measurement

Capillary end effect was another issue that influenced the previous unsteady experiment. In the current experiments, some new pressure ports were drilled along the fracture for intermediate pressure difference measurement to minimize capillary end effect and facilitate intermediate absolute pressure measurement through the fracture. Another issue that affects the pressure measurement is the phase transformation inside the pressure tubing. Since experiments were conducted at a temperature close to boiling point of water, the water-filled pressure tubing connected to the pressure transducers has a tendency to boil. This means both liquid water and gas would coexist inside the pressure tubing. This situation can be illustrated in Figure 1.20. Insensitive and erratic pressure response was obtained due to the different compressibility in water and gas and the solubility of gas. An additional outer cooling tubing was added to cool down the pressure tubing to minimize this two-phase phenomenon inside the pressure tubing. This cooling tubing is expected to quench the pressure tubing and maintain the content inside the pressure tubing in the liquid phase (water). The new plumbing of the pressure measurement is shown in Figure 1.21. The complete improved measurement configuration in the fracture apparatus is shown in Figure 1.22(a) and (b).

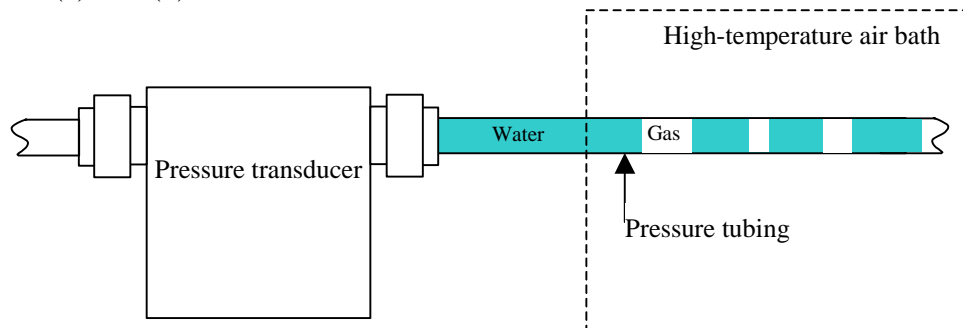


Figure 1.20: Two-phase problem inside the pressure tubing.

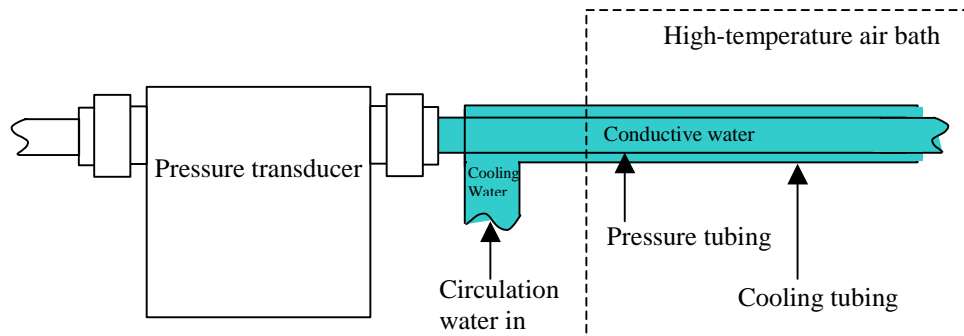
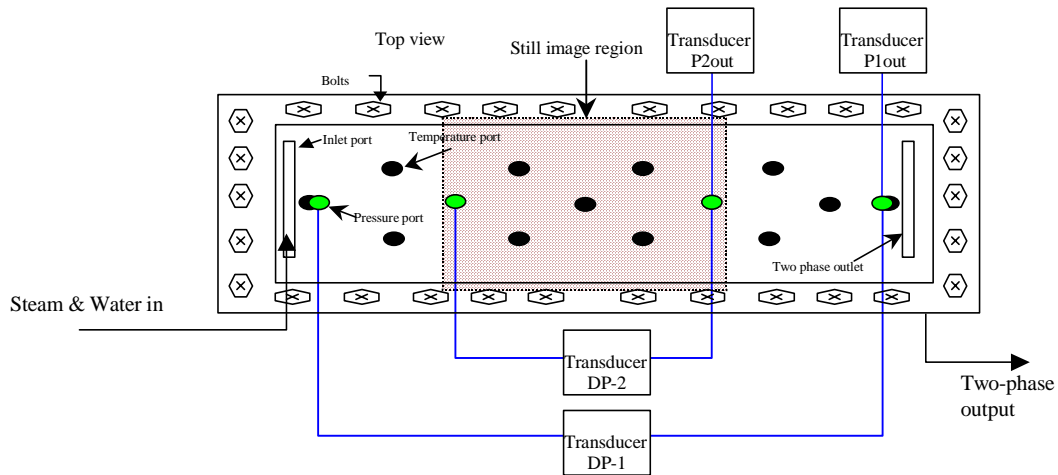
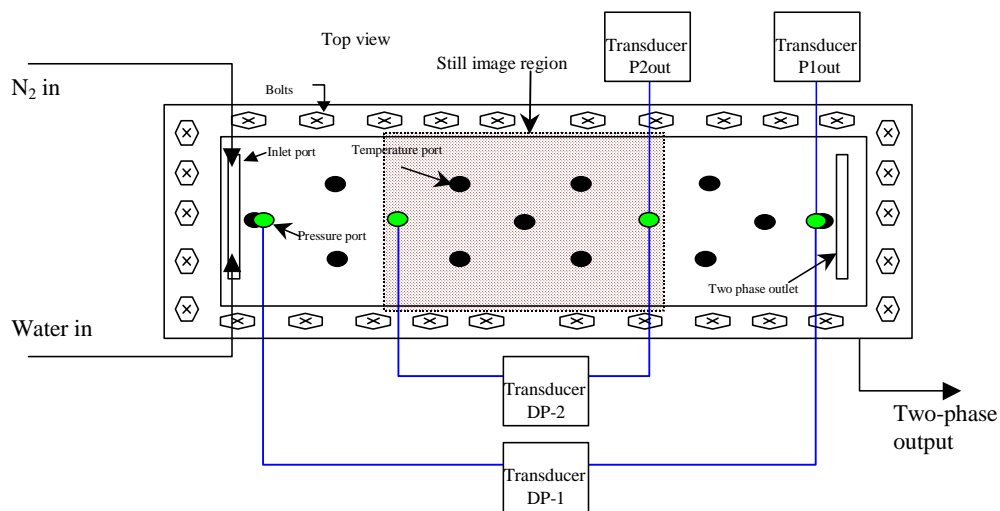


Figure 1.21: Improved plumbing of the pressure measurement to reduce two-phase problem shown in Figure 1.20.



(a) Steam-water steady experiments.



(b) Nitrogen-water steady experiments.

Figure 1.22: Schematic diagrams of pressure measurements in fracture apparatus in steady experiments. (a) Steam-water steady experiments. (b) Nitrogen-water steady experiments.

Still images will be taken both over the whole fracture region and in the intermediate region shown in Figure 1.22. Comparison of relative permeabilities obtained from these two flow regimes will be made to characterize the magnitude of the capillary end effect and flow stability.

1.5 PRELIMINARY RESULTS

A steady-state nitrogen-water relative permeability experiment at 90°C is under way. From several runs of this experiment, the nitrogen-water flow behavior at high temperature behaves similar to that at room temperature. The latter was conducted by Diomampo (2001) in the same fracture. The gas forms its own flow path through the fracture. This flow path undergoes continuous snapping and reforming due to the invasion of water. Figure 1.23 shows four consecutive images taken during eight seconds. As can be seen in these four images, the gas flow path is nearly stable except some gas flow patterns that are blocked (part 3 and 4 in Figure 1.23(c) and (d)), and some that are unblocked (part 1 and 2 in Figure 1.23(c) and (d)). These pictures were taken at a gas rate of 25 ml/min and water rate of 3 ml/min. Comparing Figure 1.23 to Figure 1.4 (previous steam-water result), even at high temperature conditions, nitrogen-water flow still forms a nearly stable flow path. However, steam-water flow never forms any stable flow path for any phase. This difference is probably the major reason causing the difference between steam-water and nitrogen-water relative permeability as shown in Figure 1.7. The whole experiment is still in progress.

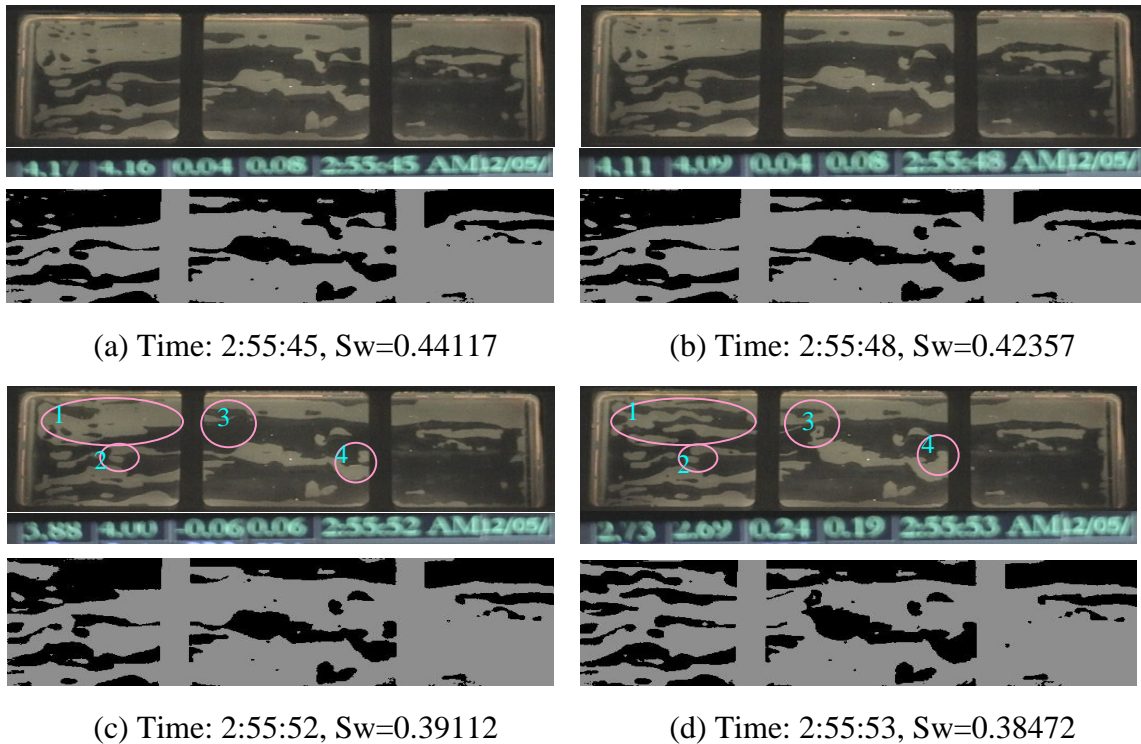


Figure 1.23: The continuous nitrogen-water flow behavior in smooth-walled fracture at 90°C, gas rate= 25 ml/min, water rate= 3 ml/min.

2. NUMERICAL SIMULATION WITHOUT USING EXPERIMENTAL RELATIVE PERMEABILITY

This research project is being conducted by Senior Research Engineer Kewen Li and Professor Roland Horne. The objective of this project is to develop a numerical simulation technique without using experimental relative permeability data for geothermal reservoir engineering.

2.1 SUMMARY

This study proposes a numerical simulation approach without direct specification of relative permeability functions from experimental data. Using this approach, it is not necessary to impose relative permeability functions as input to the simulator in order to conduct the numerical simulations of two-phase fluid flow such as steam-water flow in geothermal reservoirs. Instead only capillary pressure data need to be imposed and the relative permeabilities can be calculated consistently using specific models. Example numerical simulations at both core and reservoir scales were conducted to test the technique without the direct input of relative permeability functions from experimental data. The results showed that the production performance calculating from the numerical simulations without the input of relative permeability functions was almost the same as the experimental data. Using the method proposed in this study, the effects of pore size distribution index and entry capillary pressure on recovery by gravity drainage were investigated at both core scale and reservoir scale. The technique may be especially suitable for geothermal reservoirs in which it is difficult to measure relative permeability curves. The proposed technique may also be useful to upscaling, numerical simulation while drilling, and other areas.

2.2 INTRODUCTION

Reducing uncertainty (Zhang *et al.*, 2000; Hastings *et al.*, 2001; Caldwell and Heather, 2001) has been a challenge for the past decade or so in numerical simulation and reservoir engineering. One source of prediction uncertainty is that the input to numerical simulators is uncertain and inaccurate. For example, relative permeability data variation may introduce significant uncertainty. Pickup *et al.* (2000) reported recently that variation in relative permeability due to small-scale heterogeneities, such as cross-bedding, could have a significant impact on reservoir performance. On the other hand, experimental data of relative permeability may also have significant error or uncertainty. McPhee and Arthur (1994) reported a comparison study in which homogeneous core samples were provided to five different laboratories and specific procedures were specified. It was found that residual saturation could vary by 20% and there was a great difference between the highest and lowest end point water relative permeability values. If the laboratories applied their own standard analysis procedures, the discrepancies in residual saturation increased to about 34% and the discrepancies in relative permeability might be unacceptable. Due to the great uncertainty from experimental data, relative permeability is often a parameter set to tune or obtain by automatic history match. However, tuning the relative permeability parameters independently may result in curves that are unphysical and/or inconsistent with other flow properties.

Uncertainty may be reduced if the number of input parameters is decreased, especially if the parameters with greatest uncertainty are avoided. This may be realized by imposing only capillary pressure data as input to numerical simulators. Relative permeability can be inferred because relative permeability and capillary pressure are correlated. There are many papers in this field. Purcell (1949) developed a method to calculate the permeability using pore size distribution derived from mercury-injection capillary pressure curves. This method established the relationship between permeability and capillary pressure. Later the relationship was extended to multiphase fluid flow in porous media and was used to calculate relative permeabilities, as reported by Gates and Leits (1950). After that, Burdine (1953) introduced a tortuosity factor in the model. Corey (1954) and Brooks and Corey (1966) summarized the previous works and modified the method by representing capillary pressure curve as a power law function of the wetting phase saturation. Honarpour *et al.* (1986) reviewed the literature on the correlation between relative permeability and capillary pressure in drainage cases in this field. Land (1968, 1971) established the relationship between relative permeability and capillary pressure in imbibition cases.

Papatzacos and Skjæveland (2002) reported a theory for single-component, two-phase flow in porous media. The theory includes wettability and capillary pressure as integral parts of the thermodynamic description and does not make use of the relative permeability concept. However, by providing a capillary pressure correlation, it is possible to infer relative permeabilities.

Capillary pressure and relative permeability are important input to numerical simulation. Even though it was found long ago that both are correlated, the experimental data of capillary pressure and relative permeability are usually still imposed as two separate inputs to numerical simulators.

Recently we demonstrated that relative permeabilities in many two-phase fluid flow systems, including steam-water flow, could be calculated satisfactorily using specific models once reliable capillary pressure data are available (Li and Horne, 2002). According to this finding, it may not be necessary to impose relative permeability functions as separate input to the simulator in order to conduct the numerical simulations of two-phase fluid flow. Instead only capillary pressure data need to be imposed and the relative permeabilities can be calculated using the models that we specified in a previous paper (Li and Horne, 2002). There are many advantages to doing so. Measurements of relative permeabilities over the full range of saturation are usually time-consuming, expensive, and inaccurate in many cases while the measurements of capillary pressure curves are faster, cheaper, and more accurate. Reservoir engineering computations may be more efficient, more economical, more consistent, and more reliable by using the capillary pressure methods to obtain relative permeabilities instead of using separate specification in the simulator input.

On the other hand, the correlation between capillary pressure and rock properties has been established experimentally much better than that between relative permeability and rock

properties. Unlike the common method (tuning relative permeability curves), one can match production history by tuning capillary pressure curves with physical significance based on the well-established correlation between capillary pressure and rock properties (J -function). One more advantage is that uncertainty may be reduced because the number of input parameters is decreased.

In this study we conducted example numerical simulations using the approach proposed. The results demonstrated that the production calculated by imposing only the capillary pressure data is consistent with the experimental data. The relative permeabilities required for numerical simulation were calculated from the experimental data of capillary pressure. We also showed that the proposed numerical simulation approach would be useful to conduct theoretical study or sensitivity analysis by numerical simulation. For example, the effects of entry capillary pressure and pore size distribution index on recovery were investigated at both core and reservoir scales.

2.3 THEORY

In a previous paper (Li and Horne, 2002), we demonstrated that relative permeability of two-phase fluid flow could be calculated satisfactorily using reliable capillary pressure data in a series of specific cases. The Brooks and Corey model (1966) has been accepted widely to calculate relative permeability using capillary pressure data. However the Purcell model (1949) was found to be the best fit to the experimental data of the wetting phase relative permeability in many cases. The differences between the experimental and the Purcell model data for the wetting phase were almost negligible. We concluded in the previous paper (Li and Horne, 2002) that the wetting phase relative permeability could be calculated using the Purcell model (1949) and the nonwetting phase relative permeability could be calculated using the Brooks-Corey model (1966). According to this finding, the wetting phase relative permeability can be calculated accurately using the following equation:

$$k_{rw} = (S_w^*)^{\frac{2+\lambda}{\lambda}} \quad (2-1)$$

where k_{rw} and S_w^* are the relative permeability and the normalized saturation of the wetting phase; λ is the pore size distribution index.

Eq. 2-1 was derived by substituting the following capillary pressure model into the Purcell model (1949):

$$P_c = p_e (S_w^*)^{-1/\lambda} \quad (2-2)$$

where p_e is the entry capillary pressure. The normalized saturation of the wetting phase in drainage cases is calculated as follows:

$$S_w^* = \frac{S_w - S_{wr}}{1 - S_{wr}} \quad (2-3)$$

where S_w and S_{wr} are the specific saturation and the residual saturation of the wetting phase.

For the nonwetting phase, relative permeability can be calculated accurately using the Brooks-Corey model (1966) as follows:

$$k_{rnw} = (1 - S_w^*)^2 [1 - (S_w^*)^{\frac{2+\lambda}{\lambda}}] \quad (2-4)$$

where k_{rnw} is the relative permeability of the nonwetting phase. Eq. 2-4 was obtained by substituting Eq. 2-2 into the Burdine model (1953).

Li and Horne (2002) developed a physical model to explain the reasons to calculate the relative permeability of the wetting and the nonwetting phases in specific cases using Eqs. 2-1 and 2-4. Note that different relative permeability models may need to use in different cases. An example is discussed as follows.

It is proposed to calculate the nonwetting phase relative permeability in a fluid-rock system using the following equation:

$$k_{ro} = (S_o^*)^{\frac{2+3\lambda}{\lambda}} \quad (2-5)$$

where k_{ro} and S_o^* are the nonwetting phase relative permeability and the normalized nonwetting saturation, which is defined in this case as follows:

$$S_o^* = \frac{S_o - S_{or}}{1 - S_{or} - S_{wi}} \quad (2-6)$$

where S_o and S_{or} are the specific saturation and the residual saturation of the nonwetting phase; S_{wi} is the initial wetting phase saturation.

2.3 RESULTS

Example numerical simulations were conducted using the proposed approach. Only capillary pressure data were imposed as input to simulators. Relative permeability data required for numerical simulations were calculated from the capillary pressure data. The results are discussed in this section.

Comparison of simulation to experimental results. To demonstrate the application of the numerical simulation approach without specifying relative permeability functions from experimental data, the production data by gravity drainage from Pedrera *et al.* (2002) were used. The reason to use oil production data was the absence of similar experimental data in geothermal systems.

Fig. 2-1 shows the experimental data of recovery, by gravity drainage in a core sample positioned vertically. The 1 m long core had a permeability of 7000 md and a porosity of 41%. Pedrera *et al.* (2002) conducted gravity drainage experiments in the gas-oil-water-rock systems with different wettability. The water phase was immobile. The case studied in this paper was the strongly water-wet system with a wettability index of 1.0 and an initial water saturation of 21%.

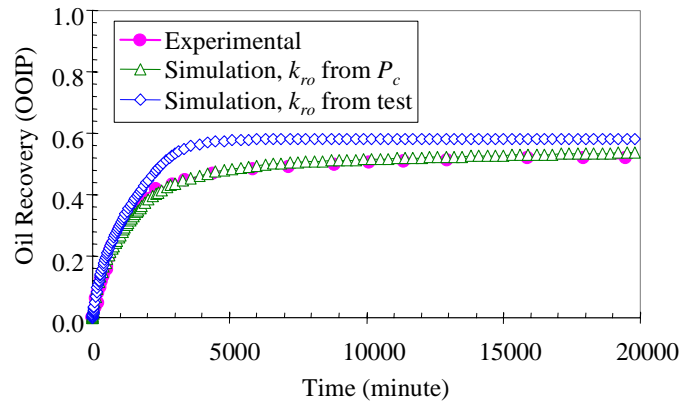


Figure 2-1: Experimental and numerical simulation data of oil recovery by gravity drainage.

The capillary pressure data obtained from the measurements of oil saturation versus the height in the core are plotted in Fig. 2-2. In order to calculate relative permeability using capillary pressure data, the Brooks-Corey model (Eq. 2-2) was used to fit the experimental data shown in Fig. 2-2. The match between the model and the experimental data is fairly good as shown in Fig. 2-2. The value of entry capillary pressure, p_{em} , obtained by fitting was 0.0259 at and λ was around 7.36.

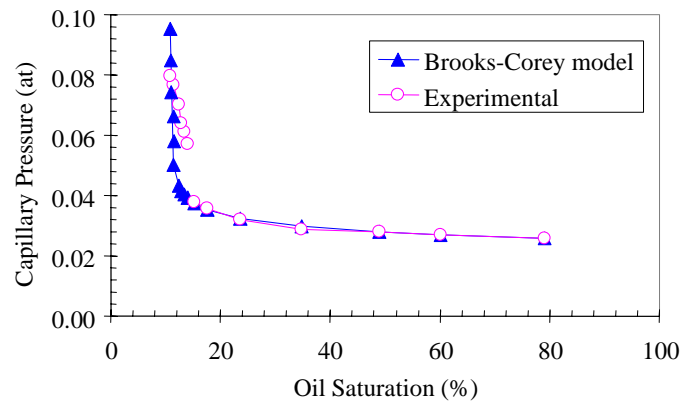


Figure 2-2: Experimental data of capillary pressure and the fitting by the Brooks-Corey model.

Gas and oil relative permeabilities were then calculated using Eqs. 2-4 and 5 with the values of p_e and λ from modeling match. The results are shown in Fig. 2-3. The reason of using Eq. 2-5 instead of Eq 1 to calculate the oil phase relative permeability is discussed in the previous section. The experimental data of the oil relative permeability data obtained by Pedrera *et al.* (2002) are also plotted in Fig. 2-3. Note that the experimental data of the oil phase relative permeability are very scattered and no gas phase relative permeability are available. It can be seen in Fig. 2-3 that the oil phase relative permeabilities calculated from the experimental capillary pressure data are approximately an average representation of the experimental data.

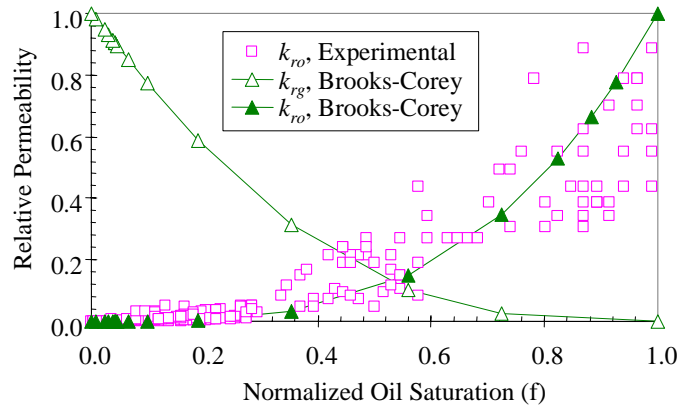


Figure 2-3: Experimental and model relative permeability data of oil and gas.

The gas and oil relative permeabilities calculated from the capillary pressure data using Eqs. 2-4 and 2-5 were used as the input data for numerical simulation. The oil recovery obtained from the numerical simulation using the model data of relative permeability instead of experimental data, represented by the open triangle symbols, is shown in Fig. 2-1. The core sample was subdivided into 100 grid blocks in the vertical direction for this one dimension problem. Fig. 2-1 shows that the oil recovery obtained from the numerical simulation using the model relative permeability data is almost the same as the experimental data (represented by the solid circles). The results in Fig. 2-1 demonstrate that it is possible to conduct numerical simulation to match oil production data correctly without using the experimental data of relative permeability, instead, using the model data calculated from capillary pressure. Using this approach, the effect of the inaccuracy and the uncertainty in the experimental data of relative permeability on the numerical simulation results may be reduced as discussed previously. For example, the experimental data of relative permeability reported by Pedrera *et al.* (2002) were very scattered as shown in Fig. 2-3. When these relative permeability data are used, the oil recovery by numerical simulation is significantly different from the experimental data. This is demonstrated in Fig. 2-1. The oil recovery by numerical simulation using measured relative permeability data (scattered) is represented by the open diamond symbols. Actually it is impossible to put this kind of relative permeability data in the simulator without any data processing because the simulator requires that oil phase relative permeability should increase with the oil phase saturation singularly. However the experimental data do not behave this way. It is

then necessary to fit the experimental data using some models, which may introduce further uncertainty.

Effect of end-point k_{rg} at core scale. The end-point gas phase relative permeability was assumed to be 1.0 in conducting the numerical simulation for the oil production by gravity drainage, which may not be true. However the gas phase mobility is usually much greater than the oil phase mobility. So the effect of the end-point gas relative permeability on the numerical simulation results may be small in some cases. To identify the effect, numerical simulations were run using different values of end-point gas relative permeability ranging from 0.1 to 1.0. The results are shown in Fig. 2-4. In this figure, k_{rg} represents the end-point gas relative permeability.

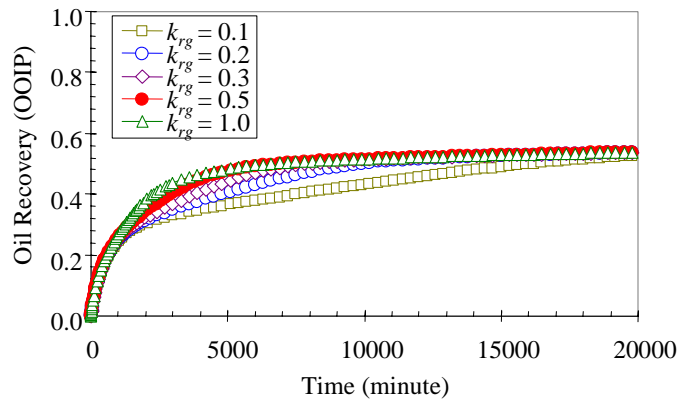


Figure 2-4: The effect of the end-point gas relative permeability on oil recovery by gravity drainage.

It can be seen that the effect of the end-point gas relative permeability on the numerical simulation results is not significant when the end-point gas relative permeability is greater than 0.5. It is estimated that the end-point gas relative permeability in the core with a permeability of 7000 md was greater than 0.5 according to the results by Gates and Leitz (1950) who reported that the end-point gas relative permeability in a core with a permeability of 1370 md was around 0.68. Therefore the value of the end-point gas relative permeability used for all the numerical simulations in this study was determined as 1.0.

Effect of λ at core scale. Gravity drainage is an important mechanism in reservoirs developed by gas injection. It has been found that unexpectedly high oil recoveries could be obtained by gravity drainage (Dumore and Schols, 1974). Capillary pressure plays an important role in both free and forced gravity drainage cases. It is essential to understand the effect of capillary pressure on the oil recovery by gravity drainage.

Capillary pressure data may be available but relative permeability data may not or may be too scattered to use, as the experimental data of relative permeability shown in Fig. 2-3. In this case, the numerical simulation approach without using experimental data of relative permeability can be used. For example, the gas-oil capillary pressure data are determined

and shown in Fig. 2-5. Note that the capillary pressure data in Fig. 2-5 are calculated using Eq. 2-2 with the same value of p_e as in Fig. 2-2 but with different values of λ ranging from 1 to 7. It is assumed that no experimental data of relative permeability are available in this case. The corresponding relative permeability data can be calculated for the different values of λ using Eq. 2-5 (note that initial water saturation resides in the rock). The results are shown in Fig. 2-6.

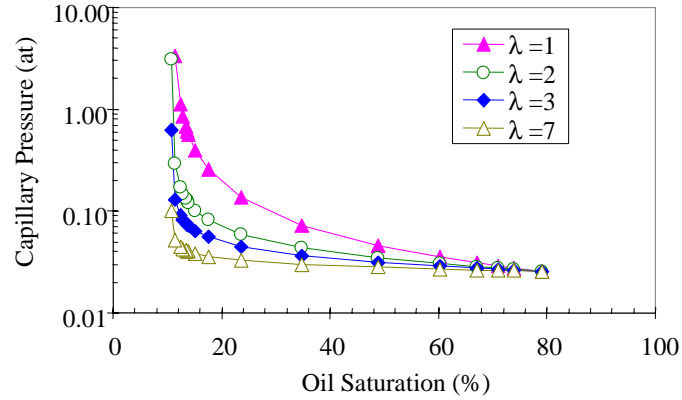


Figure 2-5: Gas-oil capillary pressure curves for different values of pore size distribution index λ .

Numerical simulations were conducted using the capillary pressure data shown in Fig. 2-5 and the derived relative permeability data in Fig. 2-6. The results are shown in Fig. 2-7. The other rock and fluid parameters are the same as used in the simulation in Fig. 2-1. Pore size distribution index λ is associated with the heterogeneity of rock at the core scale. The greater the pore size distribution index, the more homogeneous the rock. Therefore the oil recovery by gravity drainage may increase with the pore size distribution index, as shown in Fig. 2-7.

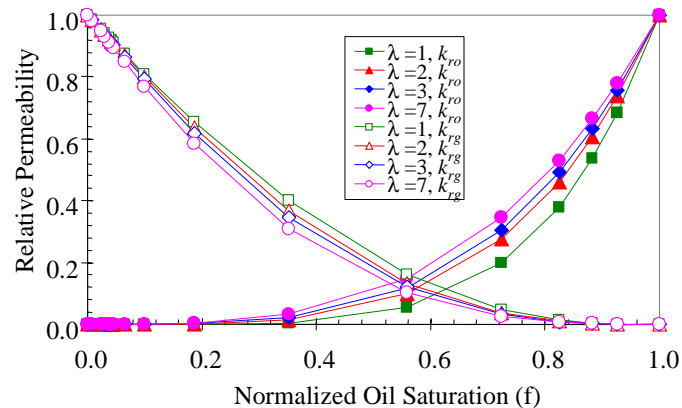


Figure 2-6: Gas-oil relative permeability curves calculated from capillary pressure data for different values of λ .

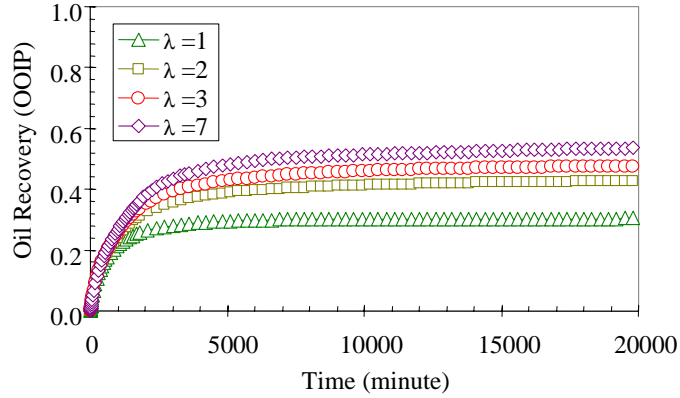


Figure 2-7: Effect of pore size distribution index on oil recovery by gravity drainage at core scale.

Effect of p_e at core scale. The entry capillary pressure is assumed constant for different values of λ in Fig. 2-5. The effect of entry capillary pressure on oil recovery may also be significant. To study this, capillary pressure curves were computed using Eq. 2-2 with different values of entry capillary pressure but with the same pore size distribution index ($\lambda=7$) in all cases. The entry capillary pressure ranged from 0.1 to 2.0 p_{em} . p_{em} is the entry capillary pressure measured by Pedrera *et al.* (2002) and used in the simulation in Fig. 2-1. The capillary pressure curves calculated using these values are shown in Fig. 2-8. Relative permeability is not a function of entry capillary pressure according to Eqs. 2-1, 2-4, and 2-5. Therefore there is only one set of relative permeability curves corresponding to the capillary pressure curves shown in Fig. 2-8. The oil and gas relative permeability curves in this case are the same as shown in Fig. 2-6 (for $\lambda=7$). The effect of entry capillary pressure on oil recovery by gravity drainage was studied by conducting numerical simulations using the capillary pressure data in Fig. 2-8 and the corresponding inferred relative permeability data. The results are shown in Fig. 2-9. The other rock and fluid parameters were the same as used in the simulation in Fig. 2-1. It can be seen that the effect of entry capillary pressure on oil recovery by gravity drainage is significant. The oil recovery by gravity drainage in the cases studied increases with the decrease in entry capillary pressure. The results demonstrate the importance of determining entry capillary pressure accurately.

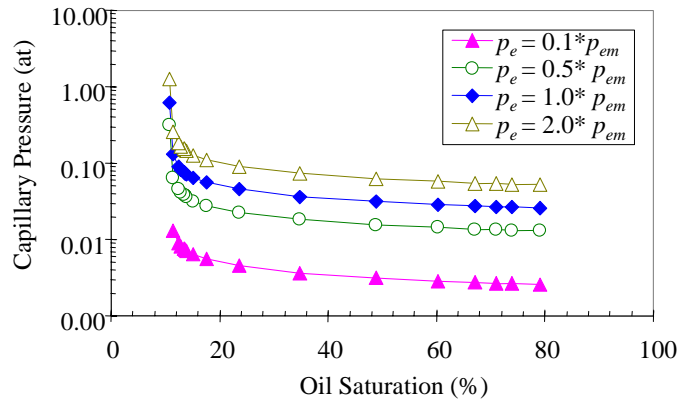


Figure 2-8: Gas-oil capillary pressure curves for different values of entry capillary pressure.

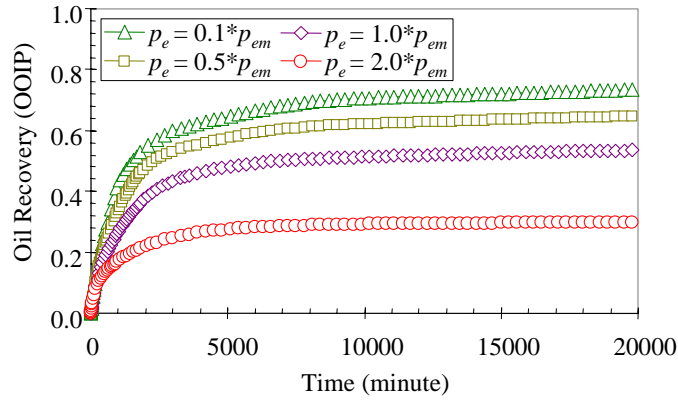


Figure 2-9: Effect of entry capillary pressure on oil recovery by gravity drainage at core scale.

On the other hand, a very limited number of capillary pressure curves are used in numerical simulations for large-scale reservoirs, even for reservoirs with great heterogeneity. It may be helpful to understand the effect of capillary pressure on oil recovery by gravity drainage at reservoir scale. This is demonstrated and discussed in the next section.

Effect of λ at reservoir scale. First a cylinder-shaped reservoir (Reservoir 1 in Table 2-1) was created according to the properties of the fluid-rock system used in the experiments reported by Pedrera *et al.* (2002). The reservoir had the same porosity (41%), permeability (7000 md), and the same initial water saturation (21%) as the core sample. The reservoir had a diameter of 200 m and a height of 50 m. It was assumed that gravity is the only driving force (free gravity drainage) for oil production in this reservoir. The values of other parameters are listed in Table 2-1. Numerical simulations were conducted using the gas-oil capillary pressure data (representing different values of λ) shown in Fig. 2-5 and the inferred relative permeability data in Fig. 2-6. The numerical simulation results for this reservoir are demonstrated in Fig. 2-10. The effect of pore size distribution index on oil recovery by gravity drainage at reservoir scale is also significant although it is smaller than that at core scale.

Table 2-1: Rock and fluid properties of reservoirs

	Reservoir 1	Reservoir 2	Reservoir 3
Permeability, md	7000	70	70
Porosity, %	41	41	41
Radius, m	100	100	100
Height, m	50	50	20
Oil density, kg/m ³	831	831	831
Gas density, kg/m ³	1.29	1.29	1.29
Oil viscosity, cp	11.3	11.3	11.3
Gas viscosity, cp	0.018	0.018	0.018
Initial water saturation, f	0.21	0.21	0.21

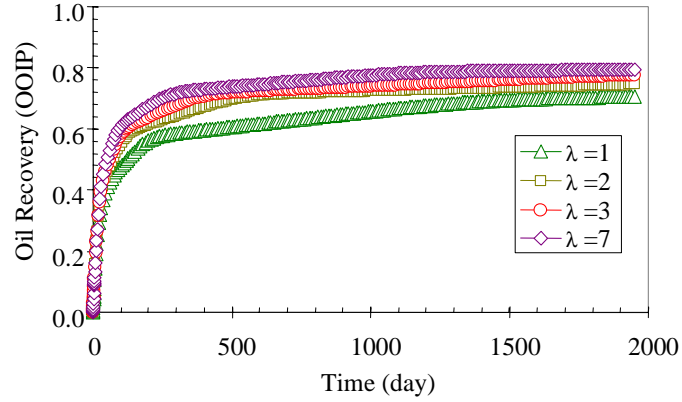


Figure 2-10: Effect of pore size distribution index on oil recovery by gravity drainage at reservoir scale in Reservoir 1 ($k=7000$ md).

To study the effect of λ on the oil recovery by gravity drainage at reservoir scale in a reservoir with a lower permeability (for example, 70 md), the corresponding capillary pressure data are required. The relationship between capillary pressure and permeability is well established. The J -function is a frequently used model to represent such a relationship, which is expressed as follows:

$$P_c = \frac{\sigma \cos \theta}{\sqrt{\frac{k}{\phi}}} J(S_w) \quad (2-7)$$

Assuming that two reservoirs have the same porosity, wettability, and the same J -function but different permeabilities, the entry capillary pressure of the reservoir (Reservoir 2, see Table 2-1) with a permeability of 70 md, p_{ec} , can be calculated from that of the reservoir with a permeability of 7000 md (p_{em}). Because the two reservoirs also have the same fluids, the surface tension is the same too. Therefore p_{ec} is equal to $10 p_{em}$ according to Eqs. 2-2 and 2-7. The capillary pressure curves in the 70 md reservoir for different values of λ can be calculated using Eq. 2-2 with the value of p_{ec} . The results are shown in Fig. 2-11.

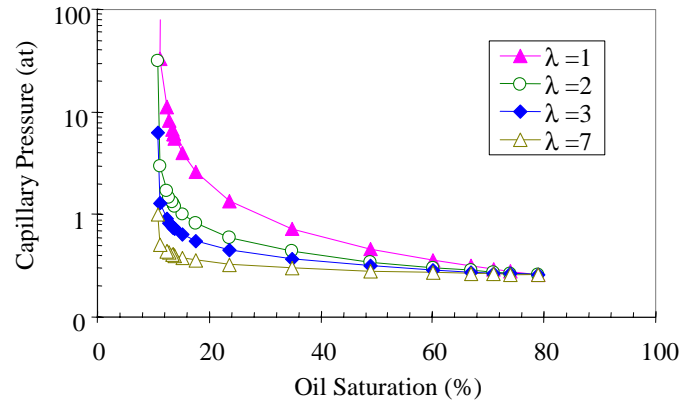


Figure 2-11: Gas-oil capillary pressure curves in rock with a permeability of 70 md but different values of λ .

Using the capillary pressure data shown in Fig. 2-11 as the input, the numerical results in the reservoir with a permeability of 70 md are obtained and shown in Fig. 2-12. Relative permeability data are the same as in Fig. 2-6 because the same values of λ are used. It can be seen that the effect of pore size distribution index on the oil recovery by gravity drainage in low permeability reservoirs is also significant after a period of production time.

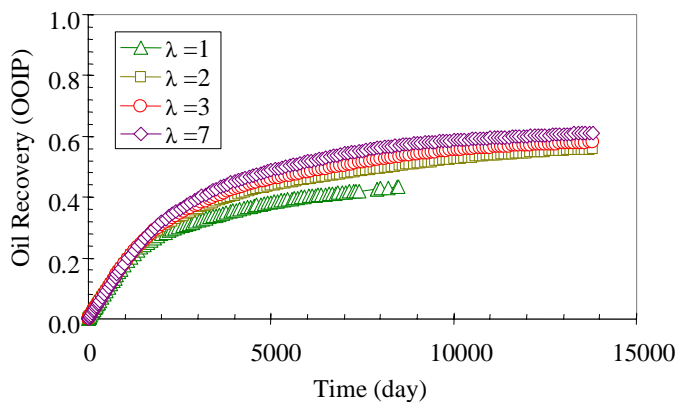


Figure 2-12: Effect of pore size distribution index on oil recovery by gravity drainage at reservoir scale in Reservoir 2 ($k=70$ md).

Effect of p_e at reservoir scale. The entry capillary pressure used to conduct the numerical simulations shown in Figs. 2-10 and 2-12 is assumed constant. To study the effect of entry capillary pressure on oil recovery by gravity drainage at reservoir scale, numerical simulations were conducted in Reservoir 1 using the capillary pressure data in Fig. 2-8. The results are shown in Fig. 2-13. There is almost no effect of entry capillary pressure on oil recovery by gravity drainage for the reservoir with a permeability of 7000 md and a height of 50 m.

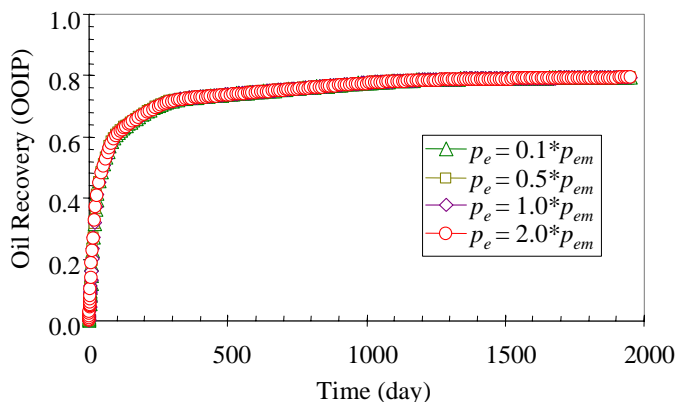


Figure 2-13: Effect of entry capillary pressure on oil recovery by gravity drainage at reservoir scale in Reservoir 1 ($k=7000$ md).

When the reservoir permeability decreases from 7000 to 70 md, the entry capillary pressure increases 10 times according to Eq. 2-7 (assuming that other parameters are

unchanged). In this case (Reservoir 2), the effect of entry capillary pressure on oil recovery by gravity drainage is greater than that in Reservoir 1, as shown in Fig. 2-14.

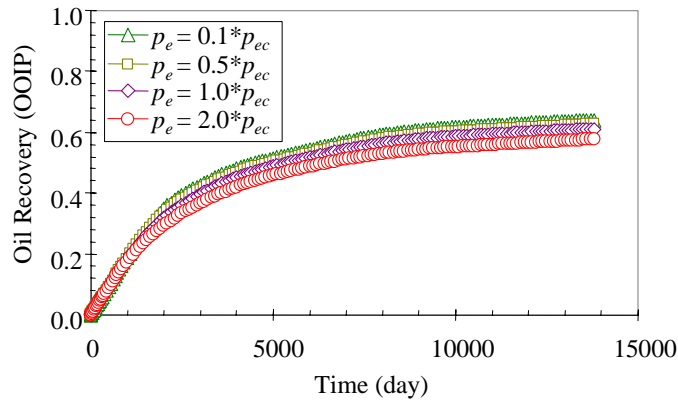


Figure 2-14: Effect of p_e on oil recovery by gravity drainage at reservoir scale in Reservoir 2 ($k=70$ md, $h=50$ m).

The effect of entry capillary pressure on oil recovery by gravity drainage also depends on reservoir height. Fig. 2-15 shows the numerical simulation results for the same reservoir as in Fig. 2-14 but with a height of 20 m (Reservoir 3), instead of 50 m. Comparing the results in Fig. 2-15 to those in Fig. 2-14, it can be seen that the effect of entry capillary pressure on oil recovery by gravity drainage is significant and greater in thin reservoirs than that in thick reservoirs.

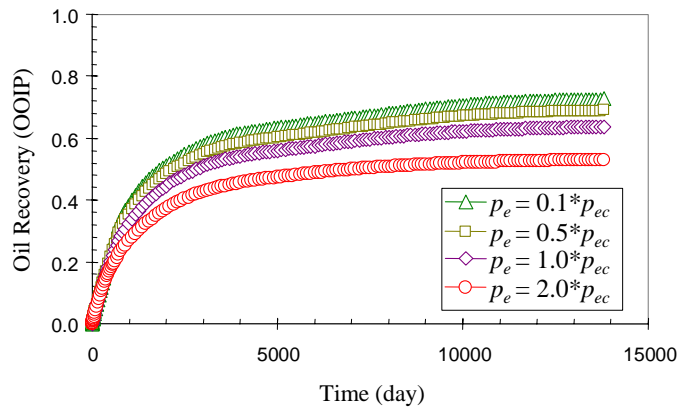


Figure 2-15: Effect of p_e on oil recovery by gravity drainage at reservoir scale in Reservoir 3 ($k=70$ md, $h=20$ m).

2.5 DISCUSSION

Since the cost of measuring relative permeability is high, the number of core samples chosen to measure relative permeability is an important consideration in the design of special core analysis. Due to this, the question of how many relative permeability measurements are required is raised. It is difficult to determine the number of relative permeability measurements technically and economically although Mohammed and Corbett (2002) proposed a method to do so. Because relative permeabilities in many two-

phase fluid flow systems can be calculated satisfactorily using capillary pressure data with specific models and the approach proposed in this paper, the answer to the question of how many relative permeability measurements are required may be zero theoretically. However, in cases in which it is technically and financially possible to measure relative permeability, we propose a few experimental measurements. The utilization of the experimental relative permeability data is to prove the validity of the specific models (for specific reservoirs) to calculate relative permeability from capillary pressure.

In conducting numerical simulations for sensitivity analysis, upscaling, and other calculations, capillary pressure and relative permeability data are often determined heuristically using empirical equations without coupling (Pickup *et al.*, 2000). However, relative permeability data can be calculated using coupled equations as discussed by Li and Horne (2002). In doing so, the data set may be more representative of actual fluid flow mechanisms in reservoirs.

The numerical simulation approach proposed in this article may be useful in many cases in which it is difficult to measure relative permeability, for example, reservoirs with extremely low permeability, geothermal reservoirs, and gas-condensate reservoirs. If the core permeability is extremely low, it takes long time to measure relative permeability and the cost will be high. In geothermal reservoirs, because of the significant mass transfer and phase transformation between two phases (steam and water) as pressure changes, it is very difficult to measure steam-water relative permeability (Sanchez and Schechter, 1990; Horne *et al.*, 2000). It is also very difficult to measure gas-condensate relative permeability curves because of the similar mass transfer and phase transformation problem (Gravier *et al.*, 1986; Chen *et al.*, 1995; Henderson *et al.*, 1995) in gas-condensate systems.

This approach may also be suitable in cases in which there is no time and no sample to conduct relative permeability measurements. Numerical simulation while drilling is such a case.

Single-phase upscaling is well understood (Renard and de Marsily, 1997), even in the near-well region (Durlofsky *et al.*, 2000; Ding, 1995). However this is not the case for multiphase upscaling, which is still a challenge (Coll *et al.*, 2001; Abtahi and Torsaeter, 1998). In many cases, reservoir permeability is upscaled but saturation dependent properties (capillary pressure and relative permeability functions) may not be. The coupling between capillary pressure and relative permeability functions and the results presented in this paper suggest that it may only be necessary to upscale the capillary pressure functions. Relative permeability functions at larger scale may be calculated from the upscaled capillary pressure functions. However, capillary pressure is often neglected in many studies regarding numerical simulation and upscaling, even for reservoirs with low permeability and great heterogeneity. If capillary pressure is neglected or assumed to be zero, relative permeability would be a linear function of fluid saturation physically. This is not the case though. It may be more representative of fluid flow mechanisms in reservoirs with low permeability and great heterogeneity to include capillary pressure in studies.

On the other hand, upscaling capillary pressure functions may be easier than upscaling relative permeability functions because of the well-established relationship between capillary pressure and rock-fluid properties. In doing so, computation cost for multiphase upscaling and uncertainty may be reduced significantly. The peculiar shapes of relative permeability curves obtained using some existing upscaling techniques might also be avoided. It is necessary yet to verify this speculation.

It seems that the numerical simulation technique proposed in this work would not be applicable in cases in which capillary pressure is negligible. However, note that relative permeability may be represented as a linear function of fluid saturation if capillary pressure is negligible. In this case, the numerical simulation approach may still be applied.

2.6 CONCLUSIONS

Based on the present study in air-water experiments, the following conclusions may be drawn:

1. Using only the experimental capillary pressure data, the production calculated from numerical simulation is almost the same as the measured experimental data. The relative permeabilities required for numerical simulation can be calculated from the capillary pressure data.
2. A numerical simulation approach was proposed without specifying relative permeability functions separately. This approach allows numerical simulations once reliable capillary pressure data are available, without the need of experimental data of relative permeability.
3. Using the approach proposed in this study, the effect of pore size distribution index on recovery by gravity drainage was investigated at both core and reservoir scales. Significant effect was observed at both scales. The recovery by gravity drainage increases with the pore size distribution index as expected.
4. The effect of entry capillary pressure on recovery by gravity drainage was also investigated. The recovery by gravity drainage increases with the decrease in entry capillary pressure, which depends on permeability, reservoir height, and other parameters.

2.7 FUTURE WORK

Similar numerical simulations in geothermal reservoirs using Tough2 will be conducted to test the approach proposed in this study.

3. REFERENCES

- Abtahi, M. and Torsaeter, O.: "Experimental and Numerical Upscaling of Two-Phase Flow in Homogeneous and Heterogeneous Porous Media", SPE 50572, presented at the 1998 SPE European Petroleum Conf., The Hague, Oct. 20-22.
- Brooks, R. H. and Corey, A. T.: "Properties of Porous Media Affecting Fluid Flow", *J. Irrig. Drain. Div.*, (1966), **6**, 61.
- Burdine, N. T.: "Relative Permeability Calculations from Pore Size Distribution Data", *Trans. AIME*, (1953), **198**, 71.
- Caldwell, R.H. and Heather, D.I.: "Characterizing Uncertainty In Oil and Gas Evaluations", SPE 68592, presented at the SPE Hydrocarbon Economics and Evaluation Symposium, Dallas, Texas, April 2-3, 2001.
- Chen, C.-Y., Diomampo, G., Li, K. and Horne, R.N.: "Steam-Water Relative Permeability in Fractures," *Geothermal Resources Council Transactions Vol.26*, 2002.
- Chen, H. L., Wilson, S. D., and Monger-McClure, T. G.: "Determination of Relative Permeability and Recovery for North Sea Gas-Condensate Reservoirs," paper SPE 30769 presented at the 1995 SPE Annual Technical Conference & Exhibition, Dallas, TX, 22-25 October.
- Coll, C., Muggeridge, A.H., and Jing, X.D.: "Regional Upscaling: A New Method to Upscale Waterflooding in Heterogeneous Reservoirs for a Range of Capillary and Gravity Effects", *SPEJ* (September 2001) **6**, 299.
- Corey, A. T.: "The Interrelation between Gas and Oil Relative Permeabilities", *Prod. Mon.*, (1954), **19**, 38.
- Ding, Y.: "Scaling Up in the Vicinity of Wells in Heterogeneous Field," SPE 29137 presented at the 1995 SPE Symposium on Reservoir Simulation, San Antonio, Texas, February 12-15.
- Diomampo, G., "Relative Permeability through Fracture", MS thesis, Stanford University, Stanford, California (2001).
- Diomampo, G., Chen, C.-Y, Li, K. and Horne, R.N.: "Relative Permeability through Fractures," *Proc. 27th Workshop on Geothermal Reservoir Engineering*, Stanford University, Stanford, California, January 28-30, 2002.
- Dumoré, J.M. and Schols, R.S.: "Drainage Capillary Pressure Function and the Influence of Connate Water", *SPEJ* (October 1974), 437.
- Durlofsky, L.J., Milliken, W.J., and Bernath, A.: "Scaleup in the Near-Well Region", *SPEJ* (March 2000) **5**, 110.
- Fourar, M. and Bories, S.,: "Experimental Study of Air-Water Two-Phase Flow Through A Fracture (Narrow Channel)," *Int. J. Multiphase Flow* Vol. 21, No. 4, (1995) pp. 621-637.

- Fourar, M., Bories., Lenormand, R., and Persoff, P.,: "Two-Phase Flow in Smooth and Rough Fractures: Measurement and Correlation by Porous-Medium and Pipe Flow Models," *Water Resources Research* Vol. 29 No. 11. November 1993, pp. 3699-3708.
- Gates, J. I. and Leitz, W. J.: "Relative Permeabilities of California Cores by the Capillary Pressure Method", presented at the API meeting, Los Angeles, California, May 11, 1950, 286.
- Gravier, J. F., Lemouzy, P., Barroux, C., and Abed, A. F.: "Determination of Gas-Condensate Relative Permeability on Whole Cores Under Reservoir Conditions," *SPEFE* (February 1986) 9.
- Hastings, J.J., Muggeridge, A.H., and Blunt, M.J.: "A New Streamline Method for Evaluating Uncertainty in Small-Scale, Two-Phase Flow Properties", SPE 66349, presented at the SPE Reservoir Simulation Symposium, Houston, Texas, February 11–14, 2001.
- Henderson, G.D., Danesh, A., Tehrani, D.H., Al-Shaidi, S., and Peden, J.M.: "Measurement and Correlation of Gas-Condensate Relative Permeability by the Steady-State Method," paper SPE 30770 presented at the 1995 Annual Technical Conference and Exhibition, Dallas, Texas, 22-25 October.
- Honarpour, M. M., Koederitz, L., and Harvey, A. H.: *Relative Permeability of Petroleum Reservoirs*, CRC press, Boca Raton, Florida, USA, 1986, ISBN 0-8493-5739-X, 19.
- Horne, R.N., Satik, C., Mahiya, G., Li, K., Ambusso, W., Tovar, R., Wang, C., and Nassori, H.: "Steam-Water Relative Permeability," Proceedings of the World Geothermal Congress, Kyushu-Tohoku, Japan, May 28-June 10, 2000.
- Kneafsy, T. J. and Pruess, K.,: "Laboratory Experiments on Heat-Driven Two-Phase Flows in Natural and Artificial Rock Fractures," *Water Resources Research* Vol. 34, No. 12, December 1998, pp. 3349-3367.
- Land, C. S.: "Calculation of Imbibition Relative Permeability for Two- and Three-Phase Flow from Rock Properties", *SPEJ*, (June 1968), 149.
- Land, C. S.: "Comparison of Calculated with Experimental Imbibition Relative Permeability", *Trans. AIME*, (1971), **251**, 419.
- Li, K., and Horne, R.N., "Accurate Measurement of Steam Flow Properties," *GRC Transactions* 23 (1999).
- Li, K. and Horne, R.N.: "Experimental Verification of Methods to Calculate Relative Permeability Using Capillary Pressure Data," SPE 76757, presented at the SPE Western Region Meeting/AAPG Pacific Section Joint Meeting held in Anchorage, Alaska, May 20-22, 2002.
- Lockhart, R. W. and Martinelli, R.C.,: "Proposed Correction of Data for Isothermal Two-Phase Component Flow in Pipes," *Chem. Eng. Prog.*, Vol. 45, No. 39, 1949.

- Mahiya, G., "Experimental Measurement of Steam-Water Relative Permeability," MS thesis, Stanford University, Stanford, California (1999).
- McPhee, C.A. and Arthur, K.G.: "Relative Permeability Measurements: An Inter-Laboratory Comparison", SPE 28826, presented at the 1994 SPE European Petroleum Conference, London, Oct 25-27, 1994.
- Mohammed, K. and Corbett, P.: "How Many Relative Permeability Measurements Do You Need?" proceedings of the 2002 International Symposium of the Society of Core Analysts, California, USA, September 22-25, 2002.
- Pan, X., Wong, R.C., and Maini, B.B.: Steady State Two-Phase Flow in a Smooth Parallel Fracture, presented at the 47th Annual Technical Meeting of the Petroleum Society in Calgary, Alberta, Canada, June 10-12, 1996.
- Papatzacos, P. and Skjæveland, S.M.: "Relative Permeability from Capillary Pressure," SPE 77540, presented at the 2002 SPE Annual Technical Conference and Exhibition, San Antonio, TX, USA, September 29 to October 02, 2002.
- Pedreña, B., Betin, H., Hamon, G., and Augustin, A.: "Wettability Effect on Oil Relative Permeability during a Gravity Drainage," SPE 77542, presented at the SPE Annual Technical Conference and Exhibition, San Antonio, TX, USA, September 29 to October 02, 2002.
- Persoff, P. K., Pruess, K., and Myer, L.: "Two-Phase Flow Visualization and Relative Permeability Measurement in Transparent Replicas of Rough-Walled Rock Fractures," *Proc. 16th Workshop on Geothermal Reservoir Engineering*, Stanford University, Stanford, California, January 23-25, 1991
- Persoff, P., and Pruess, K.: "Two-Phase Flow Visualization and Relative Permeability Measurement in Natural Rough-Walled Rock Fractures," *Water Resources Research* Vol. 31, No. 5, May, 1995, pp. 1175-1186.
- Pickup, G., Ringrose, P.S. and Sharif, A.: "Steady-State Upscaling: From Lamina-Scale to Full-Field Model", *SPEJ* (June 2000) **5**, 208.
- Pruess, K., and Tsang, Y. W.: "On Two-Phase Relative Permeability and Capillary Pressure of Rough-Walled Rock Fractures," *Water Resources Research* Vol. 26 No. 9, September 1990, pp 1915-1926.
- Purcell, W.R.: "Capillary Pressures-Their Measurement Using Mercury and the Calculation of Permeability", *Trans. AIME*, (1949), **186**, 39.
- Renard, P. and de Marsily, G.: "Calculating Equivalent Permeability: A Review," *Adv. in Water Resour.* (1997) **20**, 253.
- Sanchez, J.M. and Schechter, R.S.: "Comparison of Two-Phase Flow of Steam/Water through an Unconsolidated Permeable Medium," *SPEE*, (Aug. 1990), 293-300.
- Scheidegger, A.E. *The Physics of Flow Through Porous Media*, 3rd ed., University of Toronto, Toronto. 1974.

- Su, G. W., Geller, J. T., Pruess, K. and Wen, F.: " Experimental Studies of Water Seepage and Intermittent Flow in Unsaturated, Rough-Walled Fractures," *Water Resources Research*, Vol. 35, No. 4, April 1999, pp. 1019-1037.
- Witherspoon, P.A., Wang, J.S.W., Iwai, K. and Gale, J.E.: " Validity of Cubic Law for Fluid Flow in a Deformable Rock Fracture," *Water Resources Research*, Vol. 16, No. 6, 1980, pp 1016-1024.
- Zhang, D., Li, L., and Tchelepi, H.A.: "Stochastic Formulation for Uncertainty Analysis of Two-Phase Flow in Heterogeneous Reservoirs", *SPEJ* (March 2000) **5**, 60.